First publ. in: Laser Cleaning / ed. Boris Luk'yanchuk. New Jersey : World Scientific, 2002, pp. 255-310

Chapter 6

STEAM LASER CLEANING OF SILICON SURFACES: LASER-INDUCED GAS BUBBLE NUCLEATION AND EFFICIENCY MEASUREMENTS

P. Leiderer, M. Mosbacher, V. Dobler, A. Schilling, O. Yavas, B. S. Luk'yanchuk, J. Boneberg

The removal of dust particles from semiconductor surfaces requires new cleaning strategies such as Steam Laser Cleaning (SLC). It is based on laser-induced explosive evaporation of a liquid layer applied on the surface. We have investigated the laser-induced nucleation and growth of gas bubbles at silicon/water, silicon/isopropanol and silver-film/water - interfaces by light scattering and surface plasmon spectroscopy. The achieved superheating of the liquid before bubble nucleation sets in strongly depends on the substrate roughness. On rough metal films it is only about 30 K in water, compared to about 150 K on smooth silicon surfaces. Isopropanol (IPA) on smooth silicon surfaces could be heated to 116°C, corresponding to a superheating of 36 K. In combination with numerical calculations it was possible to determine the heat transfer coefficients silicon-water ($\xi = 3 \cdot 10^7$ W/m^2 K) and silicon – IPA ($\xi = 1 \cdot 10^7$ W/m^2 K). Using optical techniques we have measured the pressure wave created by the growing bubbles and the bubble growth velocities. For a quantitative study of the efficiency of SLC we deposited spherical colloidal particles on industrial silicon wafers. We observed a sharp threshold for particle removal at 110 mJ/cm^2 (laser $\lambda = 532$ nm, FWHM = 8 ns) which is independent of the size (diameter 800 nm down to 60 nm) and material of the particles and efficiencies above 90% for particle removal. On the basis of our results we discuss the validity of the existing SLC models and the perspective of the application of SLC as an industrial cleaning tool.

Keywords: Particle removal; steam laser cleaning; bubble nucleation; heat transfer coefficient, superheating

PACS: 81.65.C; 79.60.Bm; 42.62.Cf

1. Introduction

The interest in nanostructures at surfaces is growing rapidly due to the enormous importance of such structures for basic science and for applications in numerous areas like electronics, optics, data storage, sensor devices etc. As the size of such structures keeps getting smaller, the influence of contaminating dust particles, even if they are tiny, is more and more detrimental. This is in particular true for microelectronics (Hönig, 1988; Hattori, 1990; DeJule, 1998), where the typical width of the structures nowadays is already close to a hundred nanometers, and further reductions are in sight (Sematech Inc., 2000). A single dust particle of the same order of magnitude present on the surface during the chip production process can lead to a malfunction of the whole chip.

Mechanical cleaning techniques like ultrasonics, wiping and brushing, as they are presently used, are either not very efficient in removing very small particles or due to the mechanical contact give rise to new impurities by abrasion. Therefore alternative methods are very desirable (Kohli, 2002). An in principle very promising technique is the so-called "Laser Cleaning" (Bäuerle, 2000): the contaminated surface is heated by a short laser pulse, and the thermal expansion of the irradiated area, if rapid enough, is expected to kick the particle off the surface (Zapka, 1991; Tam, 1992; Engelsberg, 1993). This method is contactless, and the surface region where a dust particle is identified (e.g. by means of light scattering as in commercial wafer inspection tools) can easily be addressed in a controlled way.

It has been demonstrated that pulsed laser radiation is indeed capable of removing dust particles from a surface (Zapka, 1991; Tam, 1992; Engelsberg, 1993; Kelley, 1993; Vereecke, 1999; Halfpenny, 1999; Lu, 2000 a). Yet a closer inspection reveals that there is a great danger to modify the surface locally at the former positions of the particles, e.g. create crater-like structures (Leiderer, 2000; Lu, 2000 b, 2002; Mosbacher, 2001, 2002 a, b; Münzer, 2002). This can be ascribed to the enhancement of the incident light field in the vicinity of the particle (Luk`yanchuk, 2000, 2002; Mosbacher, 2001; Münzer, 2002). For very smooth and delicate surfaces, like those of commercial silicon wafers with an RMS roughness below 0.2 nm, this method is hence not applicable, because the surface defects generated by the cleaning process would be as serious for the further production steps as the presence of the impurity itself.

A slight modification of the cleaning procedure, however, appears to be able to solve this problem: just before the application of the laser pulse a thin liquid film is condensed on the surface, which then is evaporated explosively by the pulse, and the vapor jet carries the particle with it. This "Steam Laser Cleaning" (SLC, in contrast to the "Dry Laser Cleaning", DLC, described before), was introduced by several research groups about a decade ago (Beklemyshev, 1987; Assendel'ft, 1988 a, b; Imen, 1991; Zapka, 1991). In the following years several groups started to investigate the details of the SLC process (Park, 1994 a, b, 1996 a, b; Tam, 1995; Héroux, 1996; Boughaba, 1997; Leiderer, 1998; She, 1999; Mosbacher, 2000, 2002 a, b). The present article gives an account of the recent developments and the underlying physical phenomena of this technique.

2. Experimental

A quantitative analysis of the laser induced bubble nucleation process as well as the determination of cleaning efficiencies of SLC heavily relies on well defined, reproducible experimental boundary conditions. Therefore in this section we will describe the important aspects of our experimental setup.

2.1. Sample preparation

The preparation of samples used in bubble nucleation and SLC efficiency experiments is one of the most critical issues in the described experiments. Slight deviations in the preparation e.g. of contaminated samples may lead to results that are more difficult to interpret or even do not reflect the focused problem. In the following we will describe the preparation of the substrates and liquids used in our experiments.

Metal films on glass: In the experiments that monitored the bubble nucleation process via Surface Plasmon Spectroscopy we used thin silver films as substrate. These films are most suitable for the excitation of surface plasmons. A film of about 50 nm thickness was evaporated in high vacuum either onto the base of a heavy flint glass prism (n = 1.75 for λ = 632.8 nm) or onto a microscope slide (SCHOTT; BK7 glass). A 2 nm thick chromium interlayer was used to increase the adhesion between the silver film and the

glass prism. The films prepared in this way are *optically* smooth, yet on the nm scale are rough in comparison with silicon wafers

Industrial silicon wafers: As silicon substrate we used $\langle 100 \rangle$ industrial silicon wafers (Wacker Siltronic, Burghausen, Germany) with an RMS roughness of 0.2 nm. The wafers were cleaned in isopropanol (IPA) in an ultrasonic bath and subsequently have been dried in a nitrogen gas flow.

Water: The water used both in the bubble nucleation and SLC experiments was Millipore water. In the bubble nucleation experiments an additional 200 nm particle filter prevented the contamination of the liquid cell.

Isopropanol (IPA): The Isopropanol (2-Propanol $(CH_3)_2CHOH$), in industrial applications often abbreviated as IPA, was used as bought from the supplier. According to the supplier's specification the purity was at least 99.8%.

Contaminating particles: Most studies on laser cleaning use irregularly shaped particle contaminants (e.g. Al_2O_3, Si_3N_4) to investigate removal efficiencies. Although they may reflect the actual shape and size distribution of contaminants in a real world wafer cleaning process, they are unfavorable in experiments aimed to investigate the underlying basic processes. Therefore, we have used spherical colloidal polystyrene (PS; Interfacial Dynamics Corporation, Portland, OR 97224 USA) and SiO_2 (Bangs Laboratories Inc., Fishers, IL, USA and Duke Scientific Corp., 2463 Faber Place, Palo Alto, CA 94303, USA) particles. Their small size distribution (± 5% for PS, ± 20% for SiO_2) compared to irregular particles and their spherical shape enable studies of removal efficiencies for various well-defined sizes and facilitate future comparisons with theoretical models. Some experiments were also performed using irregularly shaped Al_2O_3 particles (SUMMIT CHEMICALS EUROPE GMBH, Düsseldorf, Germany) as contaminants.

The particles were deposited on the silicon sample by a spin coating process. After dilution with IPA (1:2500) the particle suspension was spun onto the silicon wafer (2000-3000 Rpm). By adjusting the rotation speed, the concentration of particles in the suspension and the total amount of suspension applied onto each sample we were able to prepare samples with more than 95% of isolated spheres at particle densities $\geq 10^7 - 10^8$ (depending on the particles size) per cm^2 (Mosbacher, 2000).

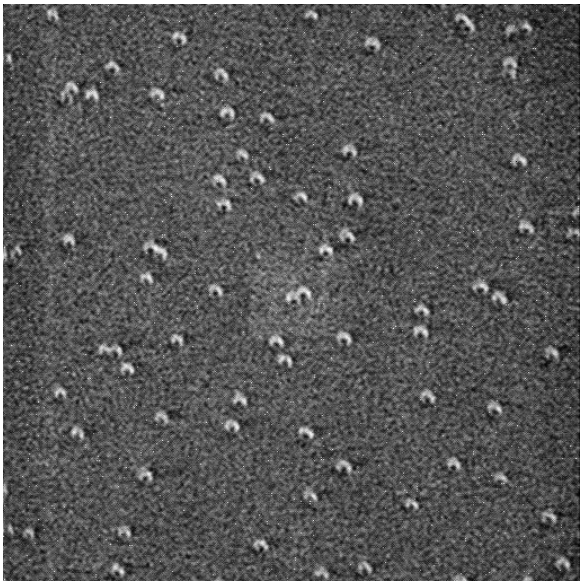

Fig.1. Typical sample as used in the laser cleaning experiments imaged in an scanning electron microscope. The displayed area is 4.8 mm × 4.8 mm and the particle size is 110 nm.

A typical example can be seen in Fig. 1 where 110 nm sized PS particles were deposited onto a Si wafer. The prevention of particle agglomerates on the samples is important for quantitative experiments, as such agglomerates complicate the interpretation of cleaning results (Halfpenny 1999) and exhibit a different cleaning behavior compared to single particles (Leiderer, 2000; She, 1999).

2.2. Laser Sources

In our experiments we applied different laser sources. For the nucleation of gas bubbles on metal substrates we have used both KrF excimer laser pulses (λ = 248 nm, FWHM = 25 ns, spot size 1 × 1 cm^2) and the pulses of a Q-switched Nd: YAG laser (λ = 532 nm, FWHM = 8 ns). As probe lasers we utilized a cw Ar -ion laser (λ = 488 nm, 175 mW) in the SLP - experiments and a HeNe - laser (λ = 633 nm, 5 mW) for the excitation of surface plasmons and the detection of contaminating particles.

2.3. Surface plasmon probe and optical reflectance probe

The experimental setup for the surface plasmon probe (SPP) of the laser-induced bubble nucleation at a liquid-solid interface is depicted in Fig. 2. After the application of the silver film, the prism is mounted on a cuvette filled with Millipore water.

Surface plasmons are excited optically at the silver-water interface via attenuated total reflection (ATR) in the Kretschmann configuration using a 5 mW HeNe probe laser (Kretschmann, 1968). Bubble nucleation takes place at the silver-water interface upon heating by a KrF excimer laser pulse through a quartz window. Any transient change of the surface plasmon resonance angle due to a change of the dielectric function of the water layer on the silver film induced by bubble nucleation, temperature rise, or pressure changes, is monitored by a fast photodiode (rise time $\leq$ 1 ns). The signal is amplified using an ac-coupled 1 GHz bandwidth amplifier, and recorded on a 500 MHz digitizing storage oscilloscope. As indicated in Fig. 2, it is calculated that the appearance of a vapor layer of 1 nm thickness will cause a significant shift of the surface plasmon resonance to a smaller angle of incidence and thus lead to a transient change in the measured intensity, if the angle of incidence of the probe laser is kept fixed. It should be pointed out here that the existence of a vapor layer is just an assumption at this point.

In order to directly compare the results of the novel SPP with the previously used optical reflectance probe (ORP), a second HeNe probe laser, incident from the front side through the liquid and probing the same spot as the SPP, is used to monitor simultaneously the transient reflectance changes caused by light scattering on bubbles.

If not stated otherwise, the SPP measurements presented in the following have been performed by setting the angle of incidence for the probe beam to the middle of the left wing of the surface plasmon resonance at about 53.1^{o} as shown in Fig. 2. In order to verify that no reversible changes of the optical constants of the silver film took place upon laser heating, the complete plasmon resonance curve has been measured prior to and after each series of experiments.

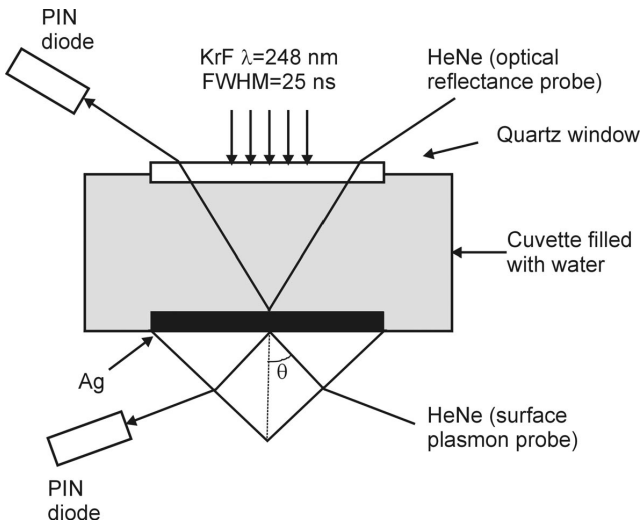

(a) Experimental setup SPP

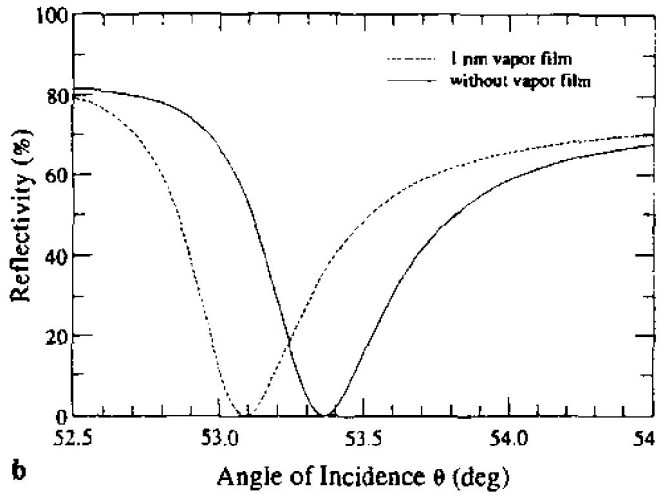

(b) Response of plasmons resonance on bubbles

Fig. 2. (a) Experimental configuration for the ns time resolved study of pulsed laser-induced bubble formation at a liquid-solid interface using the surface plasmon probe (SPP) and optical reflectance probe (ORP) techniques. (b) Calculated shift of the surface plasmon resonance curve caused by a 1 nm thick vapor layer at the water-silver interface.

2. 4. Scattered Light Probe (SLP)

Fig.3 shows the setup for the bubble nucleation experiments. In order to nucleate the bubbles a Q-switched Nd: YAG laser (λ = 532 nm, FWHM = 8 ns) heated the silicon sample. The pulse energy was split (BS) and measured for each individual pulse by an energy meter (FM: Field Master, Coherent). Sample and liquid were placed in a fused silica cuvette that could be heated up to 360 K. The growing bubbles were monitored by a cw Ar-ion laser (λ = 488nm, P = 175 mW), which was focused onto the sample.

Both the specular reflected beam of the Ar-Ion-laser and the light scattered by the nucleated bubbles were collected in forward direction (as shown in the diagram), the scattered light in addition also perpendicular to the incident ray (similar setup, not shown in the diagram). For all the light detection we used fast photodiodes (PD: FND 100, rise time < 1 ns) covered by interference filters (IF). Using a polarizing beam splitter (PBS) the reflected beam was decomposed into its p- and s-polarized constituents that were detected individually.

2. 5. Evaluation of the cleaning efficiency

In principle there are two ways of determining the cleaning efficiency of laser cleaning. Either the efficiency is evaluated on the basis of a direct observation in an optical or scanning electron microscope (Halfpenny, 1999; Lu, 2000 a; Fourrier, 2001) or by indirect probe techniques such as light scattering measurements (Mosbacher, 2000).

Recently (Mosbacher, 2000) we have compared both methods in measuring the particle removal efficiency in SLC experiments on bare silicon wafers. Direct observation and light scattering were found to provide consistent results even for particles as small as 100 nm in diameter. Therefore, we chose the light scattering approach in our experiments, as it increases the speed of data analysis.

Using a photomultiplier we were able to detect scattered light from particles with diameters down to 60 nm. The detection of the scattered light from these particles represents the detection limit of our present setup, but might be extended to even smaller sizes by the application of lasers with higher intensity and shorter wavelengths.

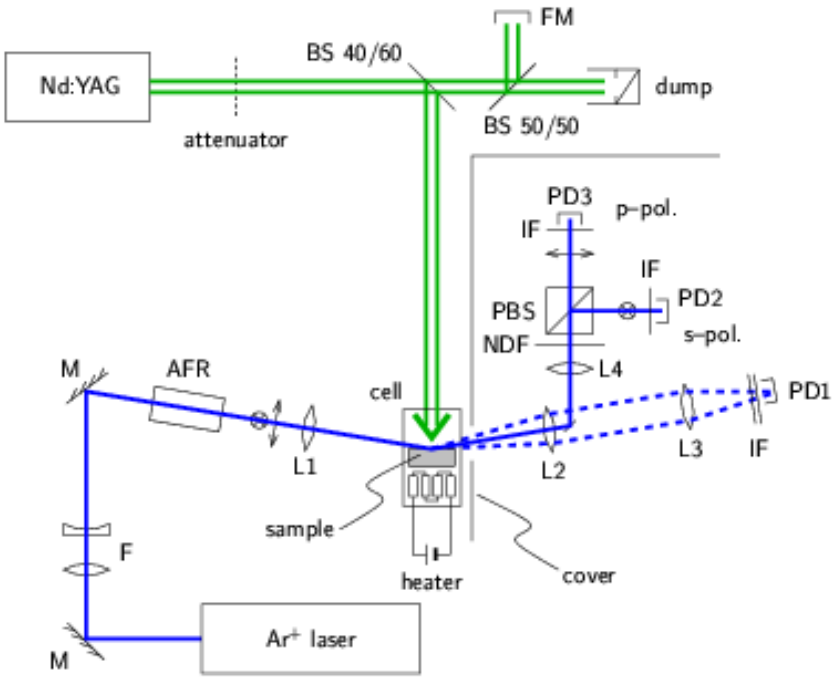

Fig. 2.3: Optical determination of laser induced bubble nucleation via Scattering light probe (SLP) (details see text).

A 5 mW HeNe laser illuminated a spot with a diameter of < 0.5 mm, which corresponds to several hundred particles at the particle concentration used. This high number of spheres ensured a small statistical error in our experiments, as we were able to monitor several hundred lifts off processes at the same time.

2.6. Determination of laser fluence

The determination of laser fluence in the SLC experiments using the Nd: YAG-laser is described in detail in (Mosbacher, 2000). In brief, the laser fluence was determined relative to the well-known (Kurz, 1983; Lowndes, 1983; Boneberg, 1993) laser fluence of about 310 mJ/cm^2 (at the laser

parameters used in the experiments) necessary for melting of a surface layer corresponding to the optical penetration depth of molten Si. In contrast to the solid state molten silicon is metallic, and hence the phase transition is accompanied by an increase in reflectivity. This increase is detected by a time-resolved monitoring of the reflected light of a HeNe laser (λ = 633 nm) during the experiment.

In the experiments designed for the determination of laser induced bubble nucleation in bulk liquids we chose another, intrinsic laser fluence calibration method. During the experiment we found a distinct change in the reflectivity of the water-silicon-system. As computer simulations of the temperature dependency of this reflectivity show, this change is primarily caused by the temperature change in the water and hence to the applied laser fluence. Based on this, it can be shown (Dobler, 2002) that the integral

$$W = \int_{4\mu s}^{9\mu s} \left(\frac{R_p(t)}{R_{0,p}} - 1 \right) dt \sim \Phi, \qquad (1)$$

containing the reflectivity change in p-direction is directly proportional to the applied laser fluence. The upper boundary of the integral is given by the limit of detection time; the lower boundary of 4 μs was chosen in a way that at this time no gas bubbles were present on the surface any more. Hence it is possible to determine from the measured reflectivity changes of the system the applied local laser fluence right at the area where the bubble nucleation is probed.

3. Laser induced bubble nucleation and pressure waves

In SLC the laser induced evaporation of the applied liquid is responsible for the ejection of the contaminating particles from the surface. Hence any deeper understanding of the SLC process requires an investigation of the laser induced bubble nucleation at the substrate - liquid interface. In this section we will both review results on the bubble growth dynamics obtained on rather rough metal films as well as recent results from experiments carried out on industrial silicon wafers.

3. 1. Theoretical background

The boiling of liquids is of great relevance for a broad variety of technical applications. Therefore a large amount of literature can be found on this topic. In contrast, there are only a few publications on the early stage of boiling, the nucleation of the gas bubbles. Below we will briefly summarize the relevant theoretical background necessary for the interpretation of our experimental results.

3.1.1. Kinetic limit of superheating

In Fig. 4 we show schematically part of the phase diagram of a one-component liquid. The vapor pressure curve separates the regions where the liquid and the vapor are the thermodynamically stable phases. This curve represents the equilibrium state of a flat liquid-vapor interface. A liquid is called superheated if its temperature (at a given pressure p) is above the temperature $T_{sat}(p)$ on the coexistence curve:

$$T(p) > T_{sat}(p). \tag{2}$$

Such a state can be achieved, e.g., by heating the liquid at constant pressure, as it is mostly done in the experiments described below and schematically indicated by the path $A \rightarrow B$ in Fig. 4. One should add that strictly speaking the pressure will in general increase by some amount due to the effects of thermal expansion. The degree of superheating which can be obtained is affected by two limits:

Thermodynamic limit (spinodal line): In a certain region of the phase diagram the liquid is intrinsically unstable, because the compressibility of the system is negative in this range. Fluctuations in density, however small they are, will therefore grow spontaneously. The boundary of this region is the so-called spinodal or thermodynamic limit of superheating $T_t(p)$ defined by thermodynamic states where

$$\left|\frac{\partial p}{\partial V}\right|_{T,n} = 0 . \tag{3}$$

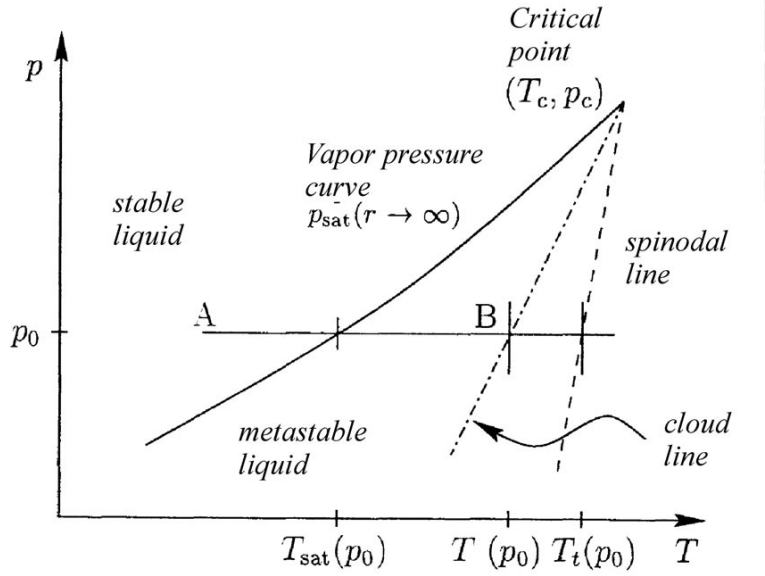

Fig. 4. Schematic *p-T* - phase diagram of a pure liquid. The path $A \to B$ corresponds to the experimentally realized isobaric heating.

The calculation of the spinodal according to equation (3) is hampered by large uncertainties, because an equation of state is required, whose parameters are not known from experiment in this range. One therefore has to rely on extrapolations (Avesisian, 1985).

Kinetic limit: In the region between the vapor pressure curve and the spinodal the liquid is in a metastable state. In this range a critical nucleus is required for the formation of growing bubbles. If a bubble is smaller than this critical size it will shrink and eventually disappear. The rate *J* of the formation of critical bubbles grows rapidly in a narrow temperature range, giving rise to a relatively sharp "cloud line" $T_{cl}(p)$ in the metastable region, where the initially transparent liquid becomes cloudy due to the enhanced light scattering from the gas bubbles (or droplets in the case of a supercooled vapor).

A review of the methods used to determine the limits of superheating and relevant data are presented in (Avesisian, 1985). The thermo-dynamics

of superheated liquids is discussed, e.g., in (Debenedetti, 1996; Skripov, 1974, 1988).

For the critical nucleation rate the typical value cited in the literature is 10^{12} $m^{-3}s^{-1}$. This is a convention. Taking into account the conditions of our experiment, with an effective volume of 50 × 20 × 0.3 mm^3 = 300 mm^3 to be probed, and a rate of one nucleus during the time of superheating (roughly 1 μs), a more adequate value is $J_{cr} = 10^{22}$ $m^{-3}s^{-1}$ in our case.

3.1.2. Nucleation theory

Nucleation of a critical nucleus in the volume of the liquid, in the absence of a wall, dust particle etc., is called homogeneous nucleation. By contrast, heterogeneous nucleation is defined as taking place at the interface between the liquid and a wall or other inhomogeneity like a dust particle. In addition there might be gas or vapor bubbles trapped in grooves or cracks of the surface, which can also act as a nucleus for growing vapor bubbles. In the following we discuss these effects and their implications (for more details, see Refs. (Avesisian, 1985; Carey, 1992; Debenedetti, 1996).

Homogeneous nucleation. The pressure p_g in a vapor bubble with equilibrium radius r_{eq} depends on the surface tension σ and the pressure in the surrounding liquid p_l via the Young-Laplace equation. From this equation it can be derived that the equilibrium radius is given by (Carey, 1992)

$$r_{eq} = \frac{2\sigma}{p_{sat}(T_l)\exp\left[v_l\left(p_l - p_{sat}(T_l)\right)/RT_l\right] - p_l}. \tag{4}$$

Here v_l is the specific volume of the liquid (assumed to be incompressible), and T_l and $p_{sat}(T_l)$ are the temperature of the liquid and the corresponding saturated vapor pressure, respectively.

An expansion of the Gibbs free energy G in a Taylor series around the equilibrium radius shows that in a superheated liquid such vapor bubbles are not stable, because $\Delta G(r)$ has a maximum at r_{eq}. This follows from the fact that for $r \to 0$ also $G(r) \to 0$, and $G(r \to \infty) < 0$ (Carey, 1992), leading to a form of $G(r)$ as shown in Fig. 5. The (unstable) equilibrium radius is

therefore also the critical radius r_{cr}: bubbles with a radius $r > r_{cr}$ grow spontaneously, whereas smaller bubbles collapse.

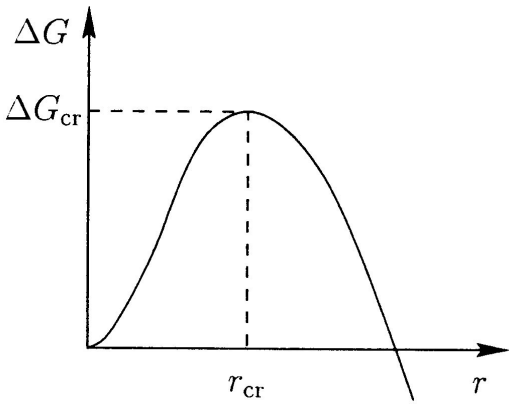

Fig. 5. Schematic representation of the Gibbs free enthalpy ΔG of a bubble as function of its radius. Bubbles nucleated in a superheated liquid grow if their radius exceeds the critical radius r_{cr}.

The number N_n^{hom} of bubbles forming spontaneously from thermally induced fluctuations in a superheated liquid with n molecules via homogeneous nucleation follows a Boltzmann distribution

$$N_n^{\text{hom}} = N_0 \exp\left[-\frac{\Delta G(r)}{k_B T}\right], \tag{5}$$

where N_0 is the number density of the molecules in the liquid. This leads to a rate J (number per volume and time) for the spontaneous formation of bubbles with the critical size r_{cr} (Avesisian, 1985; Carey, 1992) of

$$J = k_f N_0 \exp\left[-\frac{\Delta G(r_{cr})}{k_B T}\right] = k_f N_0 \exp\left[-\frac{16\pi\sigma^3}{3 k_B T_l (\eta\, p_{sat} - p_l)^2}\right]. \tag{6}$$

Here k_f denotes the molecular evaporation rate, and

$$\eta \cong \exp\left[\frac{v_l}{RT_l}\left(p_l - p_{sat}\left(T_l\right)\right)\right]. \qquad (7)$$

Hence the rate is a function of both the pressure in the liquid and the temperature T. Since the temperature-dependent quantities show up in the exponent, the nucleation rate varies quite strongly with temperature. Depending on the derivation different values for the prefactor k_f are found (Avesisian, 1985; Carey, 1992; Kagen, 1960; Katz, 1973). A comparison of the various models is given in Debenedetti, 1996. It turns out that the exact value is of minor influence on the experimentally observable nucleation threshold, because the exponential rise of the nucleation rate with superheating leads to an extremely sharp increase over many orders of magnitude within a narrow temperature interval.

Heterogeneous nucleation. Heterogeneous nucleation is the technically more important case, since liquids are most often heated via the container walls, and it is also the relevant case for SLC. The Gibbs free energy of the system is now a function of the contact angle θ of the liquid at the interface. The nucleation rate at a perfectly smooth surface can be derived in a similar way as above. Since the bubble is to be nucleated at an interface, Eq. (5) is modified to (Carey, 1992)

$$N_n^{het} = N_0^{2/3} \exp\left[-\frac{\Delta G(r)}{k_B T}\right], \qquad (8)$$

where $N_0^{2/3}$ is the number of molecules per unit area at the interface. The resulting nucleation rate J is:

$$J = \frac{N_0^{2/3}\left(1+\cos\theta\right)}{2F}\left(\frac{3F\sigma}{\pi m}\right)^{1/2} \exp\left[-\frac{16\pi F\sigma^3}{3k_B T_l\left(\eta\, p_{sat} - p_l\right)^2}\right], \qquad (9)$$

where

$$F = F(\theta) = \frac{1}{4}\left(2 + 3\cos\theta - \cos^3\theta\right). \qquad (10)$$

Once again one finds an exponential increase over many orders of magnitude in a very narrow temperature interval, giving rise to a relatively sharp nucleation threshold. Results for non-planar geometries, e.g. in and around tubes, are given in the review of Cole, 1974.

The relevant material parameters for water, namely vapor pressure $p_{sat}(T)$, surface tension $\sigma(T)$ and density $\rho(T)$, are plotted in Fig. 6. Using these values the nucleation rate $J(\theta)$ can be calculated. The results for several contact angles are shown in Fig. 7 as a function of temperature. It is obvious that the limit of superheating T_{cl} (the "cloud line" mentioned above) drops significantly for contact angles above about 80°. We note that the non-monotonous behavior of T_{cl} as a function of θ, as described by Carey, 1992, is not reproduced with the material parameters of water shown in Fig. 6.

It should also be mentioned that a description in terms of equilibrium thermodynamics, as it is given here, is strictly speaking only approximate, because nucleation of embryonic gas bubbles is a dynamic process and therefore should also be treated by a dynamic theory. Moreover, in the experiments large temperature gradients appear, which are also not included in this treatment.

Nucleation at gas bubbles. When a surface is immersed in a liquid, air or vapor bubbles can be trapped in grooves at the surface, if the contact angle of the advancing liquid θ_a is larger than the angle γ of the groove (Carey, 1992; Debenedetti, 1996). Such inclusions act as nucleation sites, when the liquid is being superheated, and vapor bubbles start growing from there. The theoretical treatment depends on the details of the groove geometry and therefore can be quite complicated. Since this situation of a rough surface is the "normal" case in technical applications, a large amount of literature exists both with respect to theory and experiment, which is only to be mentioned here (Carey, 1992; Tong, 1997)

3.2 . Experiments on metal films

Having summarized the relevant aspects of nucleation theory, we will now discuss experimental findings of laser induced bubble nucleation. First experiments in this field have been carried out on thin silver films, detecting

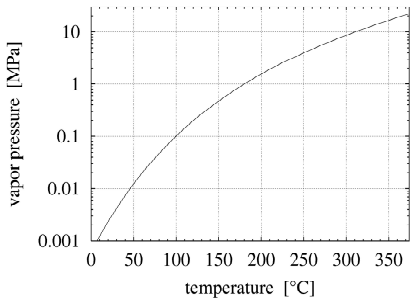

(a) vapor pressure of water

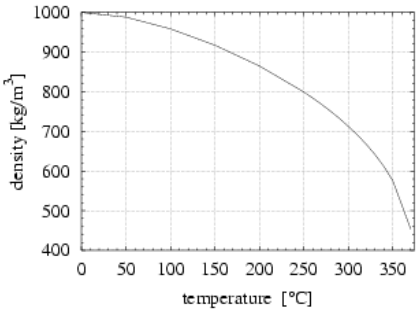

(b) density of water

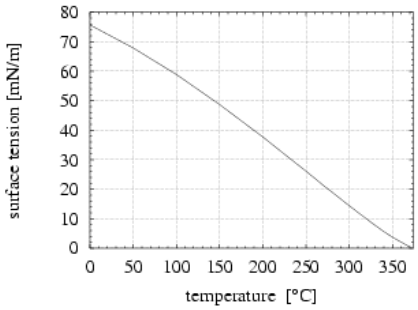

(c) surface tension of water

Fig. 6. Temperature dependent parameters for water according to (Grigull, 1984) as used in the numerical calculations.

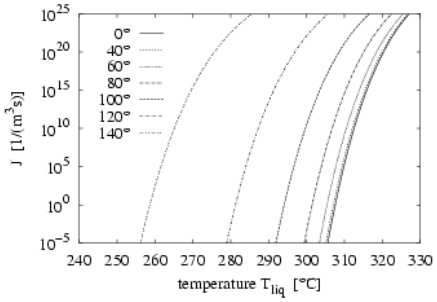

(a)

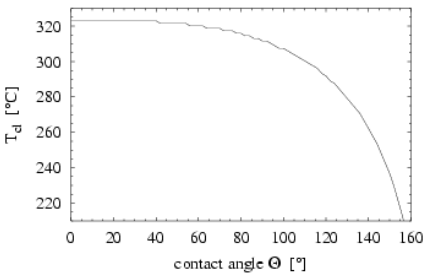

(b)

Fig.7. (a) Nucleation rate $J(\theta)$ for bubbles calculated according to Eq. (9) and using the material parameters plotted in Fig. 6. (b) Superheating temperature T_{cl} at the cloud line for a rate of $J = 10^{22}$ m^{-3}s^{-1}.

the nucleated bubbles by the optical reflectance probe (ORP) technique. The sensitivity of this technique, however, is limited to bubbles that exceed in diameter l/2. Only by the application of evanescent waves in Surface Plasmon Probe (SPP) experiments we have been able to monitor the early stage gas bubble formation. The order of the following discussion will follow the life cycle of the bubbles and therefore start with the SPP results.

3.2.1. Detection of bubble nucleation via SPP

As already mentioned, several effects may influence the position and shape of the surface plasmon resonance (Herminghaus, 1990). In order to determine the contribution of the temperature rise in the silver film, experiments have been conducted first with the bare silver film in the absence of liquid. Only a slight transient decrease in the reflected intensity is observed in this case when the laser pulse heats the film, due to the combined effect of plasmon resonance shift and broadening. However, if the experiment is carried out with a water-filled cuvette, the amplitude of the reflectance drop is drastically increased. As calculations show the change of the optical properties of the dielectric half space (in our case water) due to a given temperature rise (Schiebener, 1990) causes a much larger shift of the surface plasmon resonance than a change of the optical properties of the silver film (Johnson, 1972) induced by the same temperature rise. Consequently, the resulting shape of the surface plasmon resonance curve is predominantly governed by the changes of the refractive index of water as function of the temperature and can be used to probe the bubble growth.

Bubble nucleation threshold. As long as the laser fluence is below a certain value (which corresponds to the threshold for bubble nucleation, see below), the SPP signal exhibits no particular extra features, as shown in the topmost trace of Fig. 8a). When the excimer laser fluence is increased further, however, an additional structure in the SPP signal is observed as seen in the lower traces.

A hump in the reflectance drop starts to appear at an excimer laser fluence of $\Phi = 10.5$ mJ/cm^2, and becomes more pronounced with increasing laser fluence. The appearance of this hump can be interpreted as the onset of bubble nucleation at the water-silver interface. The surface plasmons are effectively scattered by the bubbles, and consequently the surface plasmon resonance is broadened and shifted, resulting in a temporary increase of the

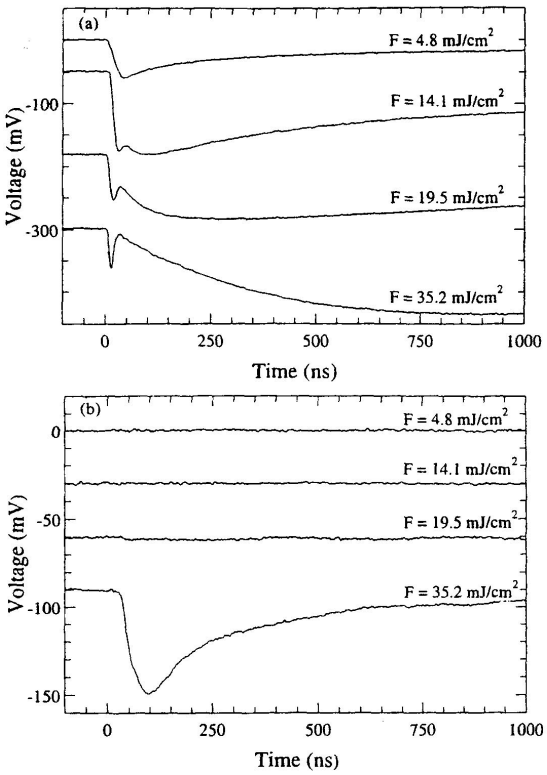

Fig. 8. (a) Surface plasmon probe (SPP) and (b) optical reflectance (ORP) signals for a water-silver interface, irradiated with increasing excimer laser fluence. 10 mV correspond to a reflectance change of 3 %. The curves are offset for clarity.

SPP intensity. When the bubbles collapse, the surface plasmon resonance becomes narrower again and the SPP signal decreases to a level, which is given by the resonance shift due to the actual temperature present at the water-silver interface.

For the laser fluence of $\Phi = 10.5$ mJ/cm^2 numerical computations based on the 1D heat transfer equation yield a peak temperature of $T = 384$ K at the water-silver interface, i.e., a surprisingly low liquid superheating of only about 10 K! This superheating is of the same order as derived for a similar system by Park, 1996. While the hump in the plasmon signal starts to appear at $\Phi = 10.5$ mJ/cm^2 and becomes more pronounced with increasing laser fluence, the simultaneously acquired reflectivity signals for ORP exhibit no particular features up to a fluence level of $\Phi = 19.5$ mJ/cm^2. Above this threshold fluence, for which computations predict a peak temperature of $T =$

473 K at the water-silver interface (liquid superheating » 100 K), a transient decrease in the ORP signal starts to appear as shown in Fig. 8b). This result clearly demonstrates the high sensitivity of the surface plasmon probe to small bubbles, which collapse before they grow up to the order of the probe beam wavelength and therefore remain invisible to the ORP.

The difference in the threshold fluences acquired using these two different methods can be explained by assuming that the threshold temperature obtained using the SPP corresponds to the temperature where bubble nucleation sets in, and the threshold temperature obtained using the ORP corresponds to the temperature where bubble growth becomes effective.

Bubble-induced pressure waves. In studies using piezoelectric transducers we have demonstrated the generation of high intensity acoustic pulses on a nanosecond time scale due to rapid bubble growth (Yavas, 1994 a, b, c). This enhancement of the acoustic pulse intensity by the rapid bubble growth process is thought to play a major role in the removal of submicroscopic particles in SLC. Since the piezoelectric transducer measurements could not provide the absolute pressure amplitudes, a quantitative data analysis was not possible with this method.

Applying the SPP, however, this quantitative information can be obtained on a nanosecond time scale (Schilling, 1996; Yavas, 1997 b). In order to eliminate any temperature effects, the experimental setup presented in Fig. 2 has been slightly modified as shown in Fig. 9. A thin quartz slide is placed in the water at a variable distance from the prism. The quartz slide is coated with 20 nm chromium and 60 nm silver on the surface facing the prism. The irradiation of the quartz slide from the rear side results in a sudden heating of the silver film and in bubble nucleation at the silver-water interface. The acoustic pulse generated during this process propagates toward the prism and can be detected by the SPP. The known relation for the dielectric constant of water as a function of pressure (Schiebener, 1990) is utilized to extract the absolute pressure amplitudes from the shift of the surface plasmon resonance curve. An example for the transient SPP signal resulting from the pulse and acquired using this setup is presented in Fig. 9.

A detailed description of the data acquisition system and the analysis of the SPP signals, i.e., conversion into absolute pressure amplitudes, is given elsewhere (Schilling, 1996; Yavas, 1997 b). The signal exhibits several peaks according to the propagation of the acoustic pulse in water and its repeated reflection between the prism and the quartz slide. The first peak

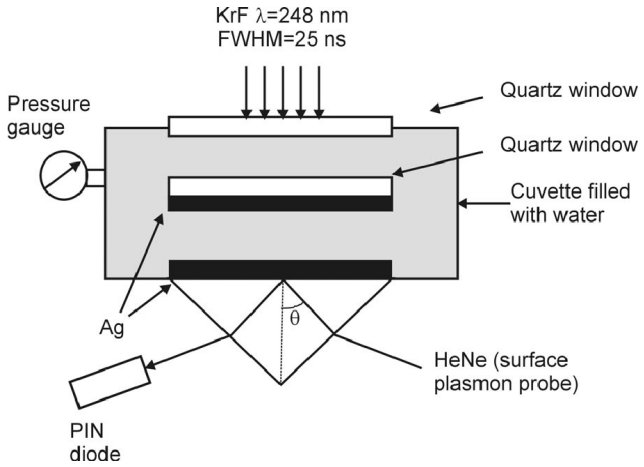

(a) Experimental setup for absolute pressure measurement using SPP

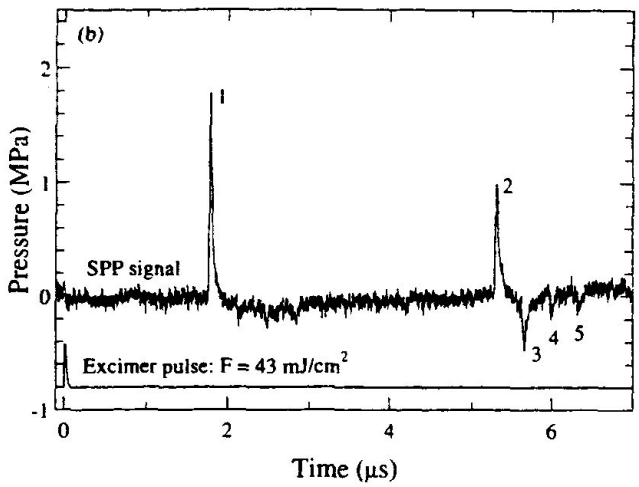

(b) Transient pressure signal

Fig. 9. (a) Experimental configuration for the absolute measurement of acoustic pulse amplitudes on a nanosecond time scale using the surface plasmon technique. In order to eliminate thermal effects on the silver film probed by SPP, the pressure is generated on the quartz slide upon excimer laser irradiation. (b) Transient pressure signal acquired using the surface plasmon probe.

corresponds to the acoustic pulse generated at the silver-water interface after its propagation to the surface plasmon detector film. The second peak represents the acoustic pulse after its round-trip between the prism and the quartz slide, reflected at the water-silver interface. Part of the acoustic pulse is transmitted into the quartz slide and is reflected back at the quartz-water interface, which is detected as the third peak in the SPP signal. Since the acoustic impedance of quartz is higher than the one of water, the reflection at the quartz-water interface leads to a phase change of π, and the compressive wave is converted into a tensile one, manifested in a negative pressure signal. The successive peaks 4 and 5 are caused by multiple reflections of the acoustic pulse in the quartz slide. By changing the distance of the quartz slide from the prism, and by using quartz slides of different thickness, we have verified that the peaks in the SPP signal represent multiple reflections of the acoustic pulse as described.

The width of the acoustic pulse is measured to be about 40 ns, which is much shorter than the previously measured pressure pulse width of » 100 ns using the photoacoustic probe beam deflection technique (Park, 1996 b) demonstrating the improved time resolution of the SPP. Due to the localized probe depth (» 200 nm), the SPP provides the real pulse profiles, while the photoacoustic deflection probe detects generally a larger pressure pulse width because of its integrating nature, i.e., the finite probe beam waist and the interaction length of the probe beam. According to our measurements the peak amplitude of the initial pulse amounts to » 2.5 MPa for the laser irradiation a laser fluence of Φ = 43 mJ/cm^2, and in the successive echoes its intensity gradually decreases due to reflection and absorption losses.

Fig. 10 displays the measured peak pressure amplitudes as function of the incident excimer laser fluence. In the plot an arrow indicates the threshold laser fluence for the onset of bubble nucleation as determined by optical reflectance probe measurements. The plot clearly demonstrates the enhanced pressure generation by rapid bubble growth. An increase in laser fluence results in an increased maximum pressure. This pressure can both result from a faster bubble growth due to a higher superheating of the liquid as well as activation of more nucleation sites and hence an increase in the number of generated bubbles. The onset of a plateau, however, indicates that in the fluence range used saturation sets in for the maximum achievable bubble size, their growth velocity and/or number density of bubbles.

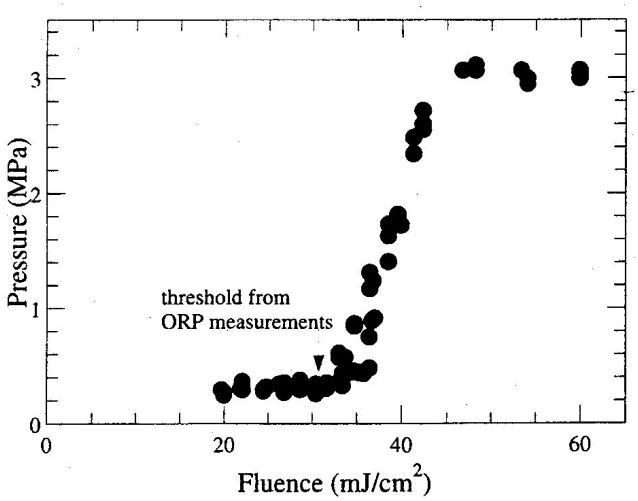

Fig. 10. Peak pressure amplitude as a function of the applied laser fluence measured by surface plasmon probe. The arrow marks the threshold for bubble growth as determined by optical reflectance probe.

Pressure amplitude of the same order of magnitude, but about two to three times lower, has been previously measured for a similar system using photoacoustic probe beam deflection and piezoelectric transducer techniques (Park, 1996 b). The discrepancy can be attributed to different samples and to the difference in temporal resolution of the test methods.

Direct proof for laser-induced bubbles. The fact that the reflection of the acoustic pulse at an acoustically less dense medium leads to a phase change, i.e., to the conversion of the compressive pulse into a tensile one, could be used to directly prove the generation of bubbles by excimer laser heating of the water-silver interface. As long as a bubble layer is present at the water-silver interface on the quartz slide, the acoustic pulse will be reflected as a tensile wave, since the reflection will take place at a water-vapor interface. When the bubbles collapse and the reflection takes place at the water-silver interface, the reflected pulse will be compressive.

This has been verified by placing a quartz slide close to the prism and successively increasing the distance after each excimer laser pulse. Representative results are depicted in Fig. 11. They clearly demonstrate the existence of bubbles up to several hundred ns after the excimer laser pulse,

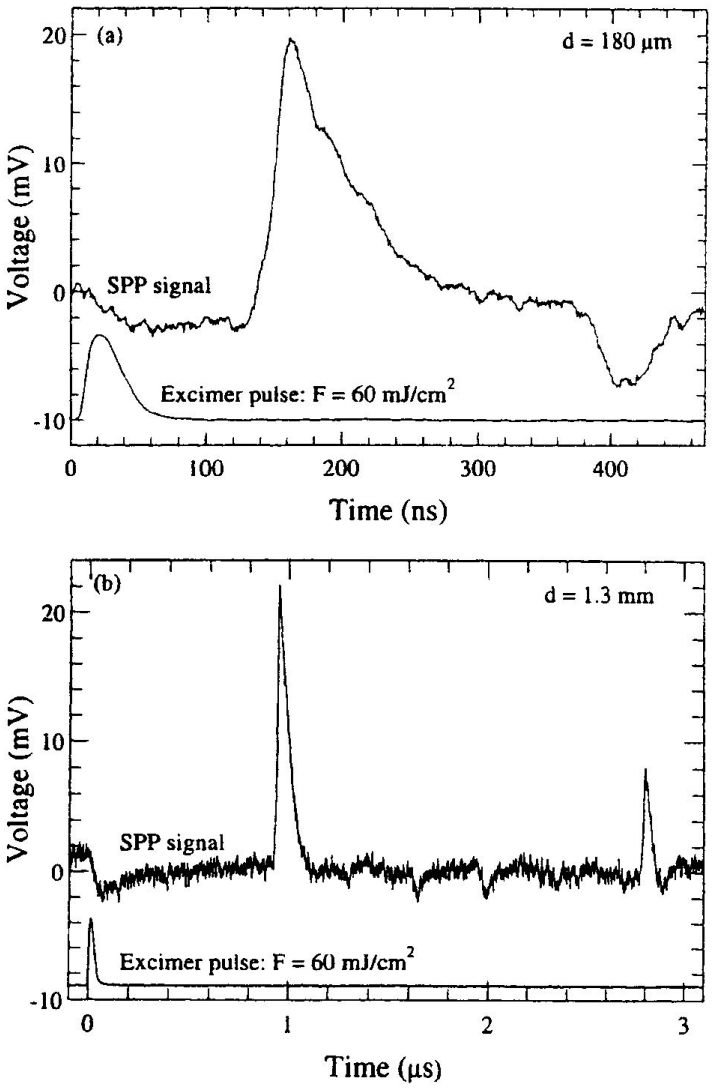

Fig. 11. (a) Direct proof of bubbles by the phase reversal of the acoustic pulse upon reflection at the water-silver interface when bubbles are present. The distance d between the two surfaces is 180 mm, and the delay time between the first and the second (in this case inverted) peak is 240 ns, corresponding to one round-trip of the acoustic pulse. (b) On a longer time scale, when the bubbles are collapsed, reflection takes place without phase reversal (d = 1.3 mm in this case).

manifested by a tensile reflected acoustic pulse. Although our previous studies already had delivered a clear evidence for laser-induced bubbles, the results presented here provide a more direct proof for such bubbles at a liquid-solid interface.

The amplitude of the reflected pressure pulse as a function of the distance d between the quartz slide and the sample surface (first echo) is plotted in Fig. 12. At d = 180 mm (the smallest distance that could be achieved experimentally), corresponding to a delay time of about 240 ns, the pressure amplitude has a negative value, as already seen in Fig. 11. As the distance is increased, the pressure peak drops in magnitude, changes sign around d = 0.5 mm, and then approaches a positive saturation value. We interpret this dependence as a gradual decrease of the bubble size and/or number, which already proceeds after 240 ns, and a complete collapse of the bubbles when the signal reaches saturation after about 1.8 μs.

Bubble growth velocities. Besides the determination of bubble nucleation thresholds the measurement of bubble growth velocities is also of great interest for the understanding of SLC. Models that predict particle as a result of shock waves generated by explosively growing gas bubbles rely on this parameter (Lu, 1999).

It is well known that the transition from Rayleigh to Mie scattering occurs at a bubble radius R_{tr} of about $\lambda_{probe} / 2\pi n_l$ (Born & Wolf, 1999). Accordingly we could use results from the optical reflectance probe experiments to determine the bubble growth velocity in excimer laser heated silver film-water systems (Yavas, 1994 c). Kim, 1996, independently confirmed the obtained value of 3.6 m/s.

Let us compare these experimental value with the one predicted by hydrodynamics. We start from the Rayleigh equation that describes the mechanical energy balance for a bubble growing in an incompressible (ρ_l = *const*) liquid (Carey, 1992):

$$R\frac{d^2R}{dt^2}+\frac{3}{2}\left(\frac{dR}{dt}\right)^2=\frac{1}{\rho_l}\left(p_v-p_\infty-\frac{2\sigma}{R}\right). \qquad (11)$$

Here p_v is the pressure of the vapor at the corresponding temperature, p_∞ is the ambient pressure and σ is the interfacial tension. In its early

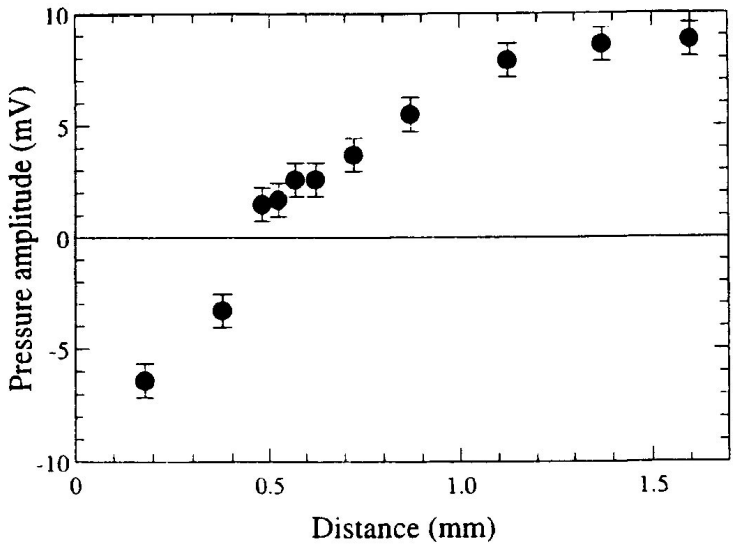

Fig. 12. The amplitude of the reflected pressure pulse as a function of the distance between the quartz slide and the SPP sample surface. Only at a distance d = 1.3 mm the signal reaches saturation, indicating that up to the round-trip time corresponding to that distance, 1.8 μs, bubbles are present after their generation by the excimer laser pulse.

stage the bubble growth is inertia-controlled and $2\sigma / R$ is much smaller than $p_v - p_\infty$. Neglecting this expression in Eq. (11) we obtain

$$R\frac{d^2R}{dt^2}+\frac{3}{2}\left(\frac{dR}{dt}\right)^2=\frac{1}{\rho_l}\left(p_v-p_\infty\right). \tag{12}$$

If one furthermore assumes that the inertial force $\propto \ddot{R}$ is negligible, one obtains the expressions for the bubble growth velocity v

$$v=\dot{R}=\sqrt{\frac{2}{3}\frac{p_v-p_\infty}{\rho_l}}, \tag{13}$$

and the maximum growth velocity v_{max}

$$v_{max} = \dot{R} = \sqrt{\frac{2}{3}\frac{p_{max} - p_\infty}{\rho_l}}\,, \tag{14}$$

that are commonly used (Yavas, 1994 b; Lu, 1999) in computations of growth velocities for the modeling of SLC. In our opinion this formula overestimates the actual situation. Inserting the experimental parameters given in (Yavas, 1994 c) results in a bubble growth velocity of about 10 m/s, about a factor of 3 larger than the experimentally determined value.

Considering the gas-bubble expansion process as a reversible one, the relation between the pressure in the vapor and the bubble radius is given by

$$p_v(R) = p_{max}\left(\frac{R_0}{R}\right)^{3\gamma}. \tag{15}$$

However, in reality the requirement of a reversible process will not be fulfilled due to the dissipation of energy via heat conduction, viscosity, etc. A thorough analysis of these dissipation processes requires the understanding of the actual dissipation mechanism and the numerical solution of hydrodynamic equations. Some of these examinations were done in the papers of (Matsumoto, 1990, 1991 a, b; Kameda, 1993). Nevertheless, a simple estimation can be obtained by merely introducing a relaxation time τ, which characterizes the dissipation. Taking into account this relaxation term and additionally considering the inertial force we derive a modified Rayleigh equation

$$R\frac{d^2R}{dt^2} + \frac{3}{2}\left(\frac{dR}{dt}\right)^2 = \frac{1}{\rho_l}\left(p_{max}\left(\frac{R_0}{R}\right)^{3\gamma} exp\left[-\frac{t}{\tau}\right] - p_\infty\right). \tag{16}$$

In this equation the adiabatic process corresponds to the limiting case of $\tau \to \infty$, whereas the non-adiabatic case is modeled via a finite value $\tau \neq 0$.

For convenience in the numerical calculations we introduced dimensionless variables into this equation. Numerically we computed the bubble growth velocities resulting from the simplified Eq. (14) and for the

cases of adiabatic and nonadiabatic vapor based on the modified Rayleigh Eq. (16). The resulting velocity as function of the normalized time is plotted in Fig. 13. From the comparison it is obvious that by considering the energy dissipation the bubble expansion velocities are reduced by a factor 2-3 compared to the simplified approach and are in good agreement with the experimental values.

3.3. Bubble nucleation on silicon wafers

Since the application of SPP in bubble nucleation studies relies inevitably on a substrate where surface plasmons can be excited, this method is not applicable to studies on silicon wafers. On the other hand, silicon wafers are the key material in semiconductor industry and SLC of these substrates is based on the laser induced bubble nucleation and explosive evaporation of the applied liquid. Hence reliable information on the bubble nucleation thresholds and bubble growth dynamics is needed not only for practical application of SLC but also for its theoretical modeling.

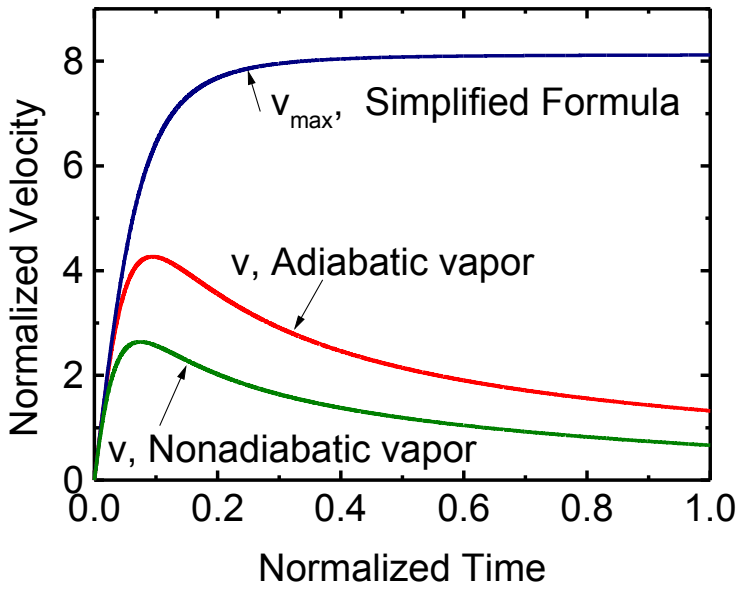

Fig. 13. Computed bubble growth velocities applying different simplifications of the Rayleigh equation.

In order to probe the bubble nucleation on silicon wafers we therefore monitored the light of an Ar-Ion probe laser that was scattered by the bubbles (SLP). The experiments on rough metal films described above revealed only small superheating of the water layer of about 10 K, compared to the theoretically predicted values at a perfectly smooth surface of about 200 K. To verify the interpretation that these results are dominated by surface roughness, we performed a series of bubble nucleation experiments on smooth substrates as well as on substrates with controlled roughness. As in an application of SLC typically mixtures of water and IPA are used, we additionally studied the bubble nucleation for the system IPA-silicon (covered by a native oxide layer).

3.3.1. Water on smooth silicon wafers

As the first system for the bubble nucleation studies we chose water (starting temperature 23 °C) on a silicon wafer (RMS roughness 0.2 nm) (Mosbacher, 2002 a).

Detecting nucleated bubbles by scattered light. Increasing step by step the pump energy delivered by the Nd: YAG laser, we first detected an increase in the system's reflectivity R for the Ar-Ion laser both for the *s*- and *p*- polarization. This can be clearly seen in Fig.14 a, where we have plotted the relative reflectivity change for both polarizations as a function of time. Within a few hundred nanoseconds the reflectivity increases and afterwards decreases during about 10 μs. Although qualitatively the signals for both polarizations do not differ, the reflectivity increase for *p*-polarization is much higher when compared to *s*-polarization. This can be explained by taking into account the initial reflectivity for the two polarizations at an angle of incidence of 82 °of the probe laser and the temperature dependence of the reflectivity values.

At moderate laser fluence no bubble nucleation took place and hence no scattered light was detected (Fig. 14 b). A slight increase in laser fluence changes this scenario. Above a certain, well-defined threshold we observed scattered light both in the plane of incidence of the probe laser (denoted by ||) and perpendicular to this plane (⊥). The scattered signals, shown in Fig. 15 b, indicate the presence of nucleated gas bubbles on the silicon surface (Yavas, 1993). After a time span of about 800 ns the scattered light

disappears, which shows that the nucleated bubbles exist for a well-defined lifetime.

Compared to the situation when laser fluence below the nucleation threshold was applied, the shape of the reflected intensity signal changes only a little. A small dip in the s-polarized intensity is the only hint on the nucleated bubbles. From this comparison it is clear that the detection of scattered light is a much more sensitive tool to monitor the dynamics of laser induced bubble nucleation and especially determine the threshold laser fluence for nucleation. Only a further increase in the applied pump laser fluence creates enough bubbles to allow bubble detection in the reflected light.

The nucleation temperature. We repeated these experiments for different starting temperatures of the water. Typical examples for the maximum of the scattered intensity as function of the applied pump laser fluence are shown in Fig. 16 for starting temperatures T_0 of 23 °C and 70 °C. Remarkable for both cases is the well-defined, sharp threshold in laser fluence, below which no bubble nucleation is detected. A comparison of this threshold for the two starting temperatures shows that for T_0 = 70 °C much less laser fluence is needed to nucleate bubbles.

This result can be interpreted in the following way: the bubble nucleation rate J increases by several orders of magnitude in a narrow temperature interval. Hence below some sharp temperature threshold of the water layer adjacent to the substrate surface no bubbles will be nucleated, whereas above this threshold many bubbles form. During the heating the liquid temperature is raised at constant pressure p_0 up to the kinetic limit of superheating $T_{cl}(p_0)$. An increase in the starting temperature of the water results in less energy ΔE that must be deposited in the liquid for heating it up to T_{cl}. In our case, this energy is deposited via heat transfer from the silicon substrate, which is heated by the pump laser. Assuming a constant heat capacity of water and silicon at the temperature intervals considered here 1 one can write for the threshold laser fluence Φ_{th}:

$$T_{cl} - T_0 \propto \Delta E \sim T_{Si} - T_0 \propto \Phi_{th}. \qquad (17)$$

In order to verify this linear dependence of Φ_{th} on the starting temperature T_0 we repeated the detection of threshold fluences for a total of

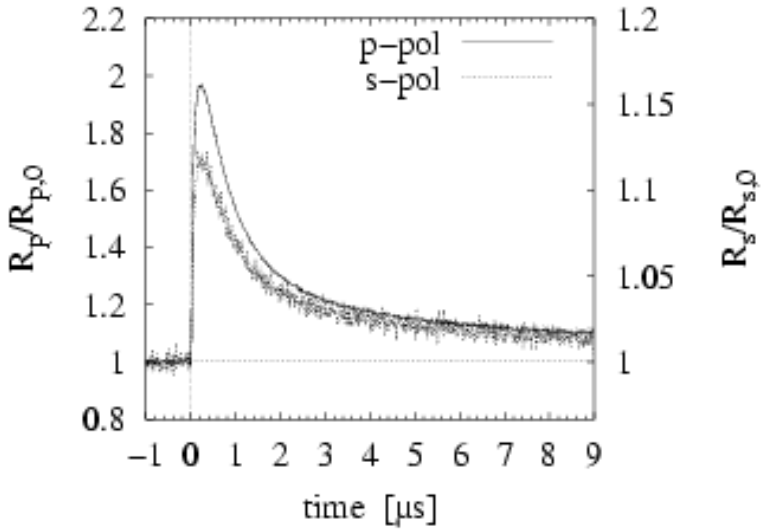

(a) Relative reflectivity for the *s*- (R_s) and *p*-polarization (R_p).

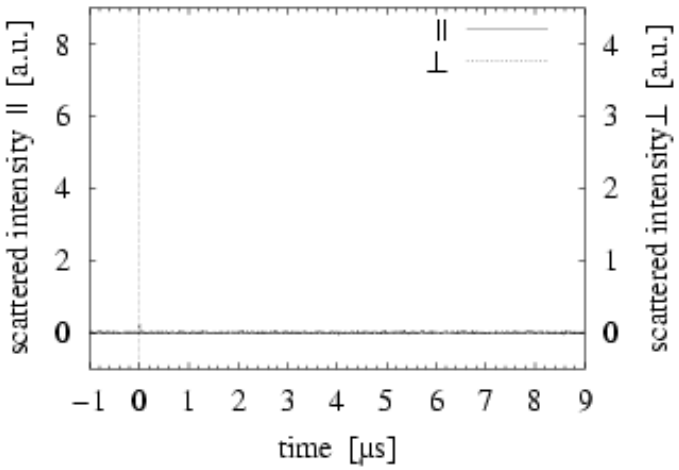

(b) Scattered intensity.

Fig.14. Detection of the reflected and scattered light intensity from a Si-H_2O interface at a laser fluence of 71 mJ/cm^2, which is below the bubble nucleation threshold.

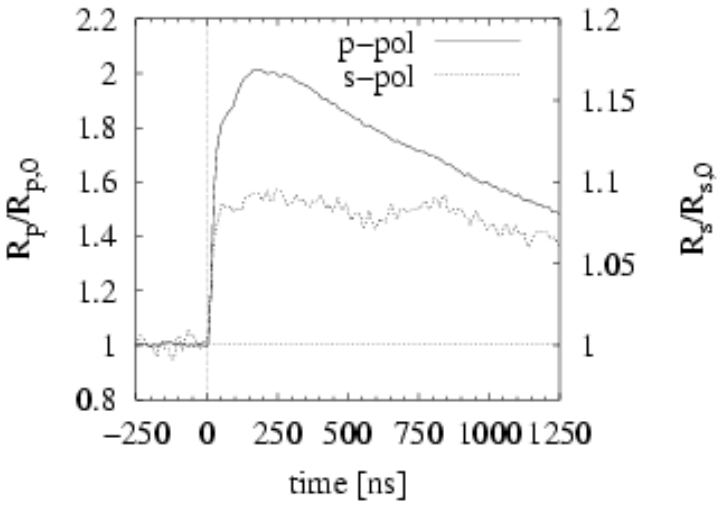

(a) Relative reflectivity for the *s*- (R_s) and *p*-polarization (R_p).

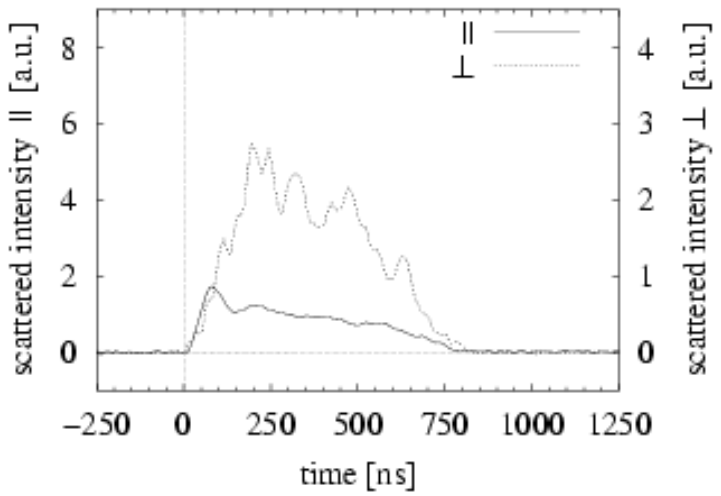

(b) Scattered intensity detected parallel and perpendicular to incident probe beam.

Fig.15. Detection of the reflected and scattered light intensity from a Si- H_2O interface at a laser fluence of 75 mJ/cm^2, which is above the bubble nucleation threshold.

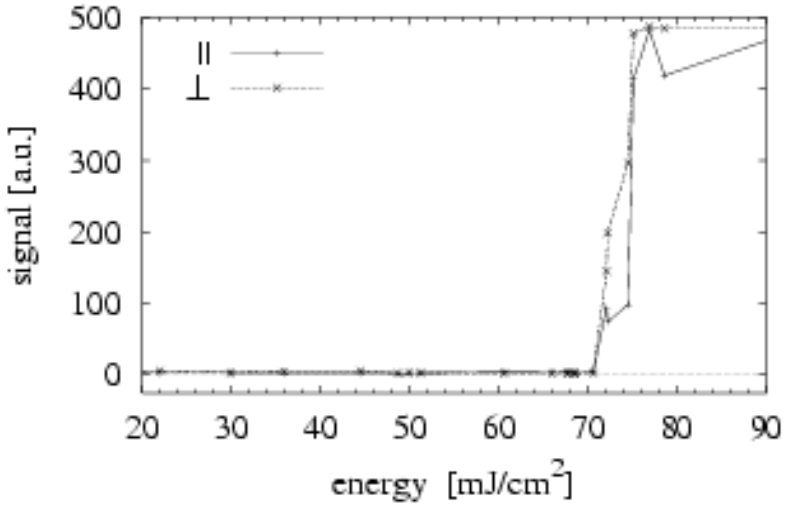

(a) Starting temperature 23 °C.

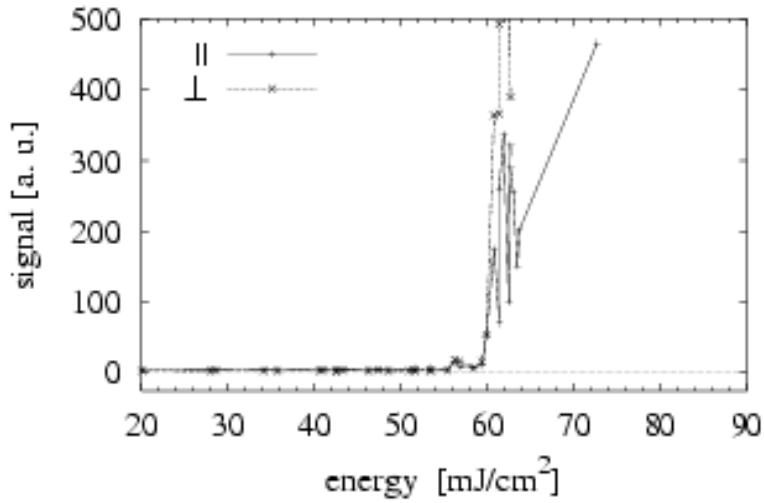

(b) Starting temperature 70 °C.

Fig. 16. Maximum scattered intensity of the probe laser as function of the applied pump laser fluence for different starting temperatures T_0 of the water. Note the well-defined, sharp threshold of bubble nucleation in laser fluence.

six more starting temperatures in the interval between room temperature and 87 °C. A plot of these results in Fig.17 clearly underlines the theoretical prediction; the threshold fluence decreases linearly from Φ_{th} = 72 mJ/cm^2 (T_0 = 23°C) to 51 mJ/cm^2 (T_0 = 87°C).

Moreover it is possible to extract the maximum superheating temperature of the water from the obtained data. If the starting temperature of water were to reach the superheating temperature present in our experiments, Eq. (17) predicts that no additional energy from the pump laser will be necessary to create gas bubbles. Hence the intersection of the linear fit of the threshold laser fluences for different starting temperatures with the x-axis of the diagram reveals the superheating temperature of the water layer. In our case the extrapolation results in a value of 250°C ± 30°C, where the error is due to the fact that the extrapolation has to be done over a large interval in temperature.

The value of 150 K ± 30 K is the first superheating temperature for laser induced bubble nucleation ever determined experimentally on a smooth substrate. Compared to the values of about 10 K measured on metal films by

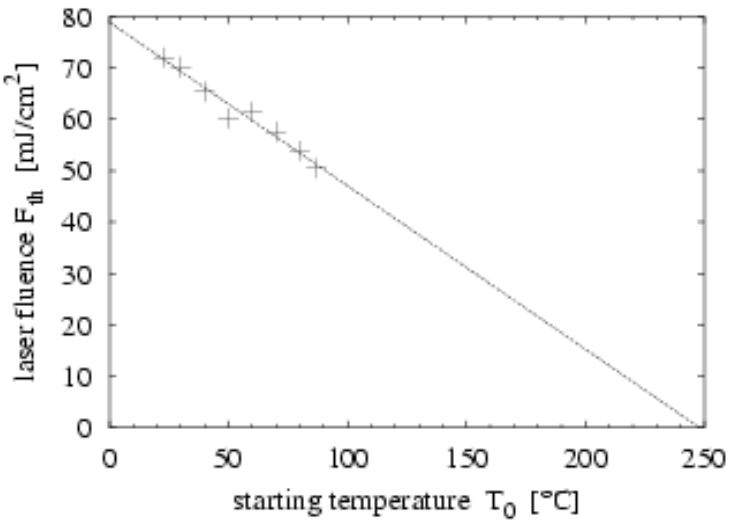

Fig. 17. Threshold fluences for laser induced bubble nucleation at a silicon/ water interface as function of the starting temperature T_0 of the water layer. An extrapolation of the linear dependence yields a superheating temperature of 250°C ± 30°C of the water.

SPP and 30 K ± 30 K determined on silver films in a control experiment using SLP, our value is much closer to the theoretical prediction of 205 K (see Fig. 7), especially if the experimental error is considered.

3.3.2. Water on structured silicon substrates

The observed high superheating values for water on smooth silicon substrates support the interpretation that the small superheating found previously for water-metal film-systems is due to the surface roughness. In order to corroborate this assertion we have performed nucleation experiments on surfaces with controlled roughness.

Silicon samples with controlled surface roughness. A controlled modification of the surface roughness of the silicon was achieved by creating well-defined holes with a diameter of a few hundred nanometers in the surface (Lu, 2000 b, 2002; Mosbacher, 2001; Münzer, 2002). For this purpose we utilized a method described in detail in (Münzer, 2002).

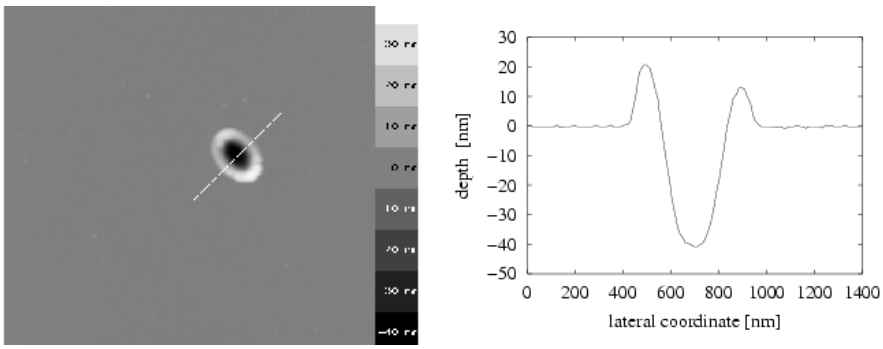

Fig. 18. A typical hole on a silicon wafer structured by nano near filed drilling as imaged by an atomic force microscope. The size of the imaged area is 3 × 3 mm^2, the white line indicates the cross section displayed in the right image.

In brief, we applied spherical PS colloidal particles 810 nm in diameter onto the substrate as described in Section 2. Illumination of the samples prepared in this way with a fs laser pulse (λ = 800 nm, FWHM = 150 fs) results in particle removal (Mosbacher, 1999, 2001) in a dry laser cleaning (DLC) process. Since for the applied laser parameters the dominating cleaning mechanism in DLC is local substrate ablation caused by the

enhancement of the applied laser fluence in the near field of the particles (Mosbacher, 2001, 2002 a) holes are created at the former position of the particles. A typical example of such a hole is shown in Fig.18. By adjusting the number density of the colloidal particles and hence the hole density on the surface we could control the roughness of the surface.

Nucleation thresholds. In the same way as discussed above for smooth silicon wafers we measured the nucleation thresholds in laser fluence for the structured substrates. A typical result obtained for T_0 = 70 ° C is shown in Fig. 19. In comparison to the results obtained on smooth surfaces the nucleation threshold is not as pronounced: the slope of the signal increase is much smaller and rather similar to the results obtained on silver films.

Nucleation temperature. Repeating the above experiment for different starting temperatures T_0 of the water, we again obtained a linear dependence of the threshold laser fluence on T_0 (see Fig. 20). Extrapolating the obtained results to vanishing fluence yields a nucleation temperature of (160 ± 13) °C. Consequently, the superheating is reduced to 60 K on these rough surfaces in comparison to the value of 150 K measured on smooth surfaces. Calling to mind the superheating of about 30 K measured by SLP on rough silver films this finding clearly confirms that the extent of superheating in laser induced bubble nucleation is dominated by the surface roughness of the substrate. The locations of roughness act as nucleation sites for the gas bubbles and are therefore responsible for the different superheating temperatures measured on the various substrates.

3.3.3 IPA on smooth silicon wafers.

As in SLC typically water/IPA - mixtures are used (Tam, 1992), we also investigated the laser induced bubble nucleation at a silicon-IPA interface. Qualitatively the results are very similar to the ones obtained for the silicon-water system. Fig. 21 shows the extrapolation of the threshold fluences in order to obtain the bubble nucleation temperature. Compared to the boiling point of 82°C the nucleation temperature of (116 ± 5) °C exhibits only a small superheating of about 30 K.

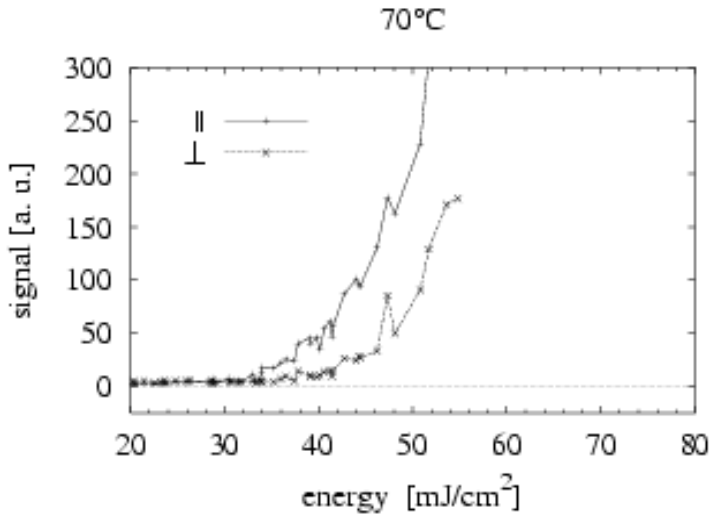

Fig. 19. Intensity of the light scattered by bubbles nucleated in water (T_0 = 70°C) on a rough silicon surface. Note that the threshold is not as sharp as for smooth surfaces.

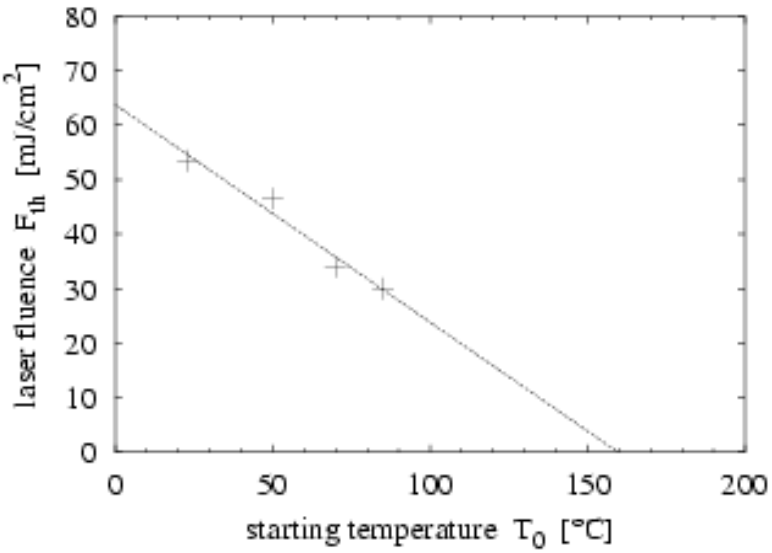

Fig.20. Threshold fluences for bubble nucleation on rough silicon surfaces as function of the start temperature T_0. The extrapolation to vanishing fluence yields a nucleation temperature of (160 ± 13) °C.

3.4. Heat transfer coefficient

It is well known that there exists a discontinuity in the temperature profile at boundaries between different materials. This is due to the finite heat conductivity of the boundary region. The so-called heat transfer coefficient

$$\xi = \frac{\dot{Q}}{A\Delta T}, \tag{18}$$

quantifies this thermal boundary resistance as a function of the heat flow $\dot{Q}$, the boundary area A and the temperature jump ΔT.

With regard to laser cleaning the thermal resistance obviously limits the heat flow from the substrate into the liquid and thus lowers the liquid temperature considerably. However, none of the published computations of temperature profiles in laser cleaning (Lu, 1999; Wu, 2000) incorporates this fact. Probably one reason is that although the phenomenon is well investigated for low temperatures below 50 K (Kapitza resistance, see Swartz, 1989) and for technical applications at room temperature, for long time scales (several seconds) and macroscopic dimensions (Nusselt-number, see Cerbe, 1999), there are no data at ns time scales and nm length scales, which would be needed for the interpretation of laser cleaning results.

The data obtained in the bubble nucleation experiments allow us now for the first time to determine the heat transfer coefficient at these scales. Fig. 22 shows computed maximum temperatures of the water layer adjacent to the silicon surface as a function of different assumed values of the heat transfer coefficient ξ between silicon and water. Our computations are based on the 1D heat equation implemented in a finite element algorithm and use temperature dependent material constants. The calculations have been done for different starting temperatures of the water and the corresponding experimentally determined laser threshold fluence for bubble nucleation was applied.

At this threshold fluence the water layer must reach the temperature T_{cl} for all starting temperatures. If the assumed value of ξ is too small or too large, however, the water layer will reach maximum temperatures that are different for each starting temperature. It can be seen from these computations that for all starting temperatures of the water the graphs of the

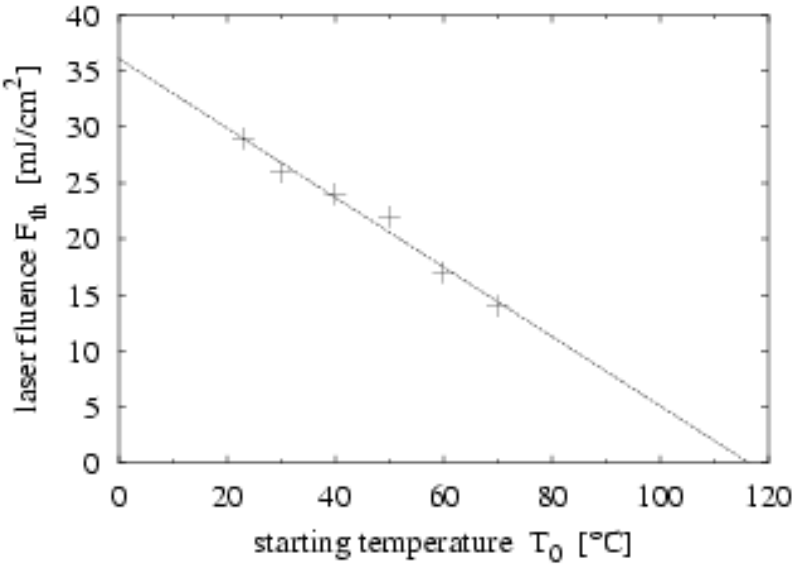

Fig. 21. Threshold fluences for bubble nucleation in IPA on smooth silicon surfaces as function of T_0. The extrapolation to vanishing fluence yields a nucleation temperature of (116 ± 5) °C.

calculated maximum temperatures as function of the assumed heat transfer coefficient intersect at one single point. This point is given by a value of $\xi_{H_2O} = 3 \cdot 10^7$ W/m^{2}K and a maximum water temperature of 250 °C - just as determined experimentally. Therefore this z-value represents the heat transfer coefficient in the studied system. Interestingly the computations exclude values of $\xi < 3 \cdot 10^6$ W/m^{2}K, as in this case the equilibrium boiling temperature of 100 °C is not reached for all starting temperatures.

In the same way we can determine the heat transfer coefficient for IPA on a smooth silicon wafer (see Fig. 23). Here the computations reveal a value of $\xi_{IPA} = 1 \cdot 10^7$ W/m^{2}K. Again, values smaller than $\xi_{IPA} = = 5 \cdot 10^6$ W/m^{2}K can be excluded as the boiling temperature is not reached for all T_0.

The ratio $\xi_{IPA}/\xi_{H_2O} = 0.33$ can be understood qualitatively in the frame of the theory of acoustic impedances. A comparison of the acoustic

impedances of IPA ($Z_{IPA} = \rho c = 0.947 \cdot 10^6$ kg/m^{2}s) and water ($Z_{H_2O} = 1.49 \cdot 106$ kg/m^{2}s) shows that the transmission probability $\alpha_{Si \to IPA}$ for a phonon at perpendicular incidence on the silicon - IPA interface is smaller than for the silicon - water system.

4. Removal of particles on surfaces via laser induced bubble nucleation: Steam Laser Cleaning

The forces exerted by the laser induced explosive evaporation can be used to remove particle contamination from surfaces. In this process called Steam Laser Cleaning (SLC) a liquid is condensed onto the surface to be cleaned and irradiated by a laser pulse. Clearly the experiments on laser induced bubble nucleation in bulk liquids described so far provide an important basis for the understanding of the SLC process. However, it should be pointed out that the bubble behavior described above is characteristic for bulk liquid rather than thin liquid films. Studies on film boiling still have to be carried out in future experiments.

4.1. Efficiency measurements

4.1.1. Dependence on the number of applied laser pulses

Clearly, with view to applications, the most interesting question in a surface cleaning process is its efficiency. More precisely, one is interested in the minimum particle size that can be removed, the percentage of particles of different size that can be removed, and in the process parameters necessary for particle removal.

As described in Section 2 we have used spherical colloidal particles made of PS and SiO_2 as model contaminants in our cleaning studies. For these particles we have determined cleaning efficiencies for a wide range of particle sizes. While varying the process parameters regarding the applied Nd: YAG laser (number of pulses, laser fluence) we have up to now not varied the liquid film properties. The film thickness was kept at a constant value in between 200 nm and 400 nm as determined by reflectometry. We also did not vary the composition of the liquid; a mixture of water (90%)

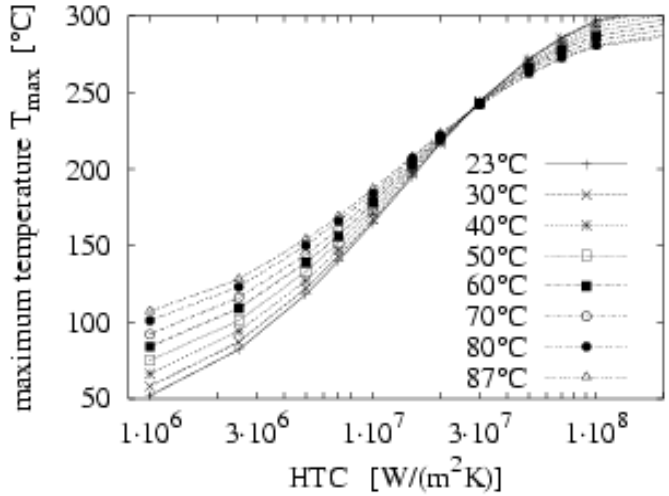

Fig. 22. Computed maximum temperatures in water on a silicon surface as function of the heat transfer coefficient (HTC) ξ_{H_2O} for different starting temperatures T_0. As laser fluence we used the experimentally determined threshold fluence for bubble nucleation.

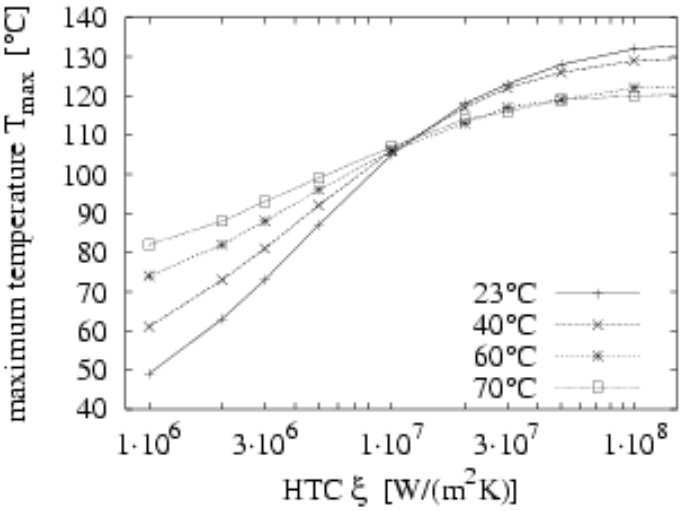

Fig.23. Computed maximum temperatures in IPA on silicon as function of the heat transfer coefficient ξ_{IPA} for different starting temperatures T_0. As laser fluence we used the threshold laser fluence.

and IPA (10%) was evaporated in all experiments.

When preparing samples with a high density of particle contaminants (average distance about 10 mm) of course one must make sure that they do not influence each other during the cleaning process. Fig. 24 shows the removal efficiency for 800 nm silica spheres as a function of laser fluence for 1, 2, 10, 20 cleaning steps. At a laser fluence of 115 mJ/cm^2 the first pulse removes only 5 percent of the particles, whereas at the somewhat increased level of 140 mJ/cm^2 already nearly half of the particles are detached under otherwise identical conditions.

If the majority of the particles is bound to the surface with the same energy, as one might expect for almost monodisperse spheres, the probability P that a particle is removed by an individual laser pulse should only depend on the applied laser fluence F and not on the previous pulses. Hence when a sequence of n pulses is applied, the fraction of remaining particles N_r / N_0 (where N_0 is the initial particle number) should be given by

$$\frac{N_r}{N_0} = (1 - P)^n . \qquad (19)$$

An analysis of the data presented in Fig. 24 indeed confirms this prediction experimentally, as demonstrated in Fig. 25, where we have plotted data for $(1 - I/I_0)$ versus the number of applied laser pulses for a laser fluence of 115 mJ/cm^2 per pulse (I_0 denotes the initial scattering intensity.) According to the argument given earlier the quantity I/I_0 is equivalent to the fraction of remaining particles. Hence $(1 - I/I_0)$ is the fraction of removed particles, which we denote in the following as "cleaning efficiency". Using Eq. (19) one expects that $(1 - I/I_0)$ should vary as $\left(1 - (1 - P)^n\right)$. The full line in Fig. 25 represents this quantity with P taken to be 0.05, as derived from the datum point for the first pulse. The agreement between the data and this line is quite satisfactory. Therefore the removal process for our samples appears to be well controlled and statistically independent for different particles, making quantitative studies feasible.

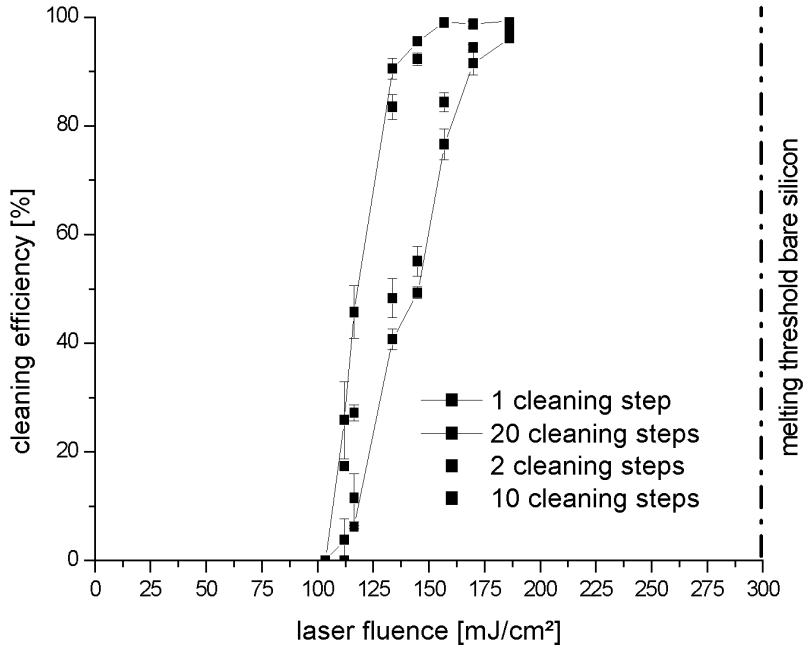

Fig. 24. Cleaning efficiency for 800 nm silica spheres as a function of laser fluence for 1, 2, 10, 20 cleaning steps.

4.1.2. Dependence on the laser fluence and variation of particle size

Results of the energy dependence of particle removal by the steam laser cleaning process for PS spheres with diameters of 800 nm, 500 nm, and 60 nm are plotted in Fig. 26. With regard to a better illustration of the cleaning behavior the results for 20 cleaning steps are plotted, which is justified by the statistically independent cleaning behavior.

For all sizes we obtain a similar behavior of the efficiency as a function of laser fluence: a steep increase in the cleaning efficiency at of $\Phi = 110$ mJ/cm^2. This absolute value of the threshold fluence was determined as described in Section 2. A comparison of the laser fluence needed for cleaning to the one necessary for melting the optical penetration depth of the silicon substrate resulted in a value of 0.35, which corresponds to above quoted threshold fluence.

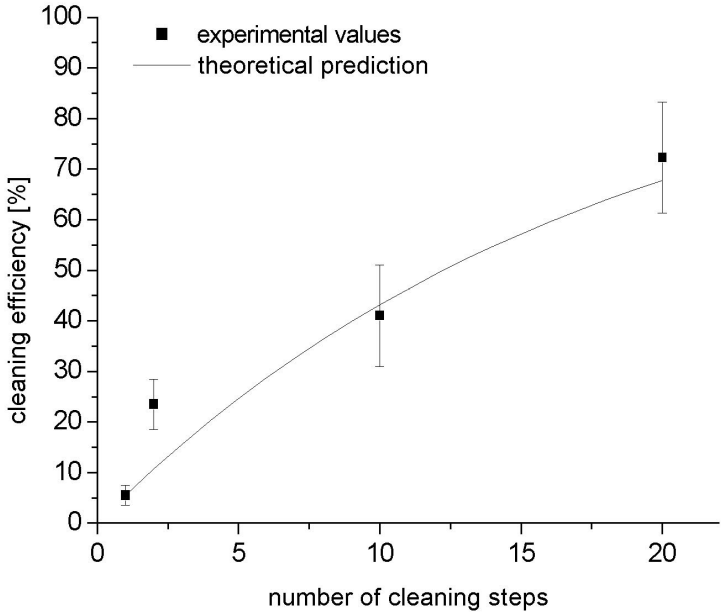

Fig. 25. Comparison of the experimental data from Fig. 24 obtained at a laser fluence of 115 mJ/cm^2 and of the theoretical value provided the particles are detached statistically independent.

The same cleaning threshold was found for PS spheres with diameters of 235 nm and 300 nm. These results are not shown in the graph for the sake of clarity. At fluences above 170 mJ/cm^2 more than 90% of the particles were removed after 20 cleaning steps (steam pulse plus laser pulse). For comparison the threshold where a (bare) Si surface would start to melt at the laser parameters used here is 270 mJ/cm^2.

In order to study the influence of the particle material on the cleaning efficiency we used silica spheres with diameters of 800 nm and 500 nm and polydisperse alumina particles with a mean diameter of 300 nm. Once again we obtain the same threshold as for PS spheres (Fig. 27) and the same dependence of the cleaning efficiency on the laser fluence. Thus the cleaning threshold is independent of both particle size and material for the investigated particles. Experiments using slightly different laser parameters (λ = 583 nm, FWHM = 2.5 ns and 7 ns as well as λ = 532 nm and FWHM = 2.5 ns) revealed again the same cleaning threshold as reported above (Mosbacher, 2000).

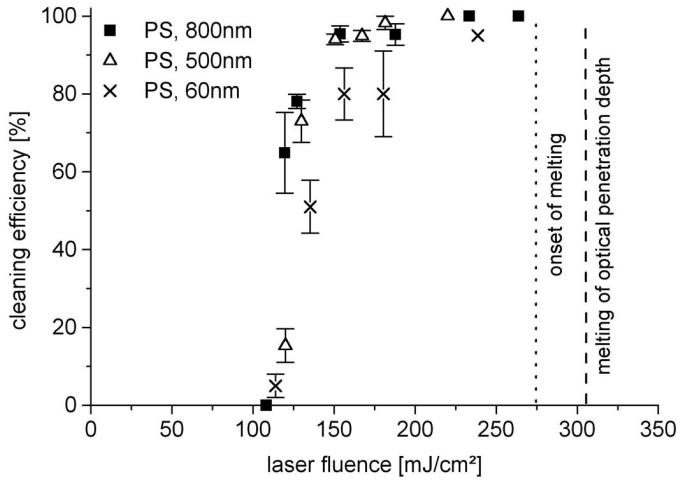

Fig. 26. Experimentally determined cleaning efficiencies as a function of applied laser fluence for various PS spheres. The cleaning threshold is size independent and the cleaning efficiency exhibits a steep increase above the onset of cleaning.

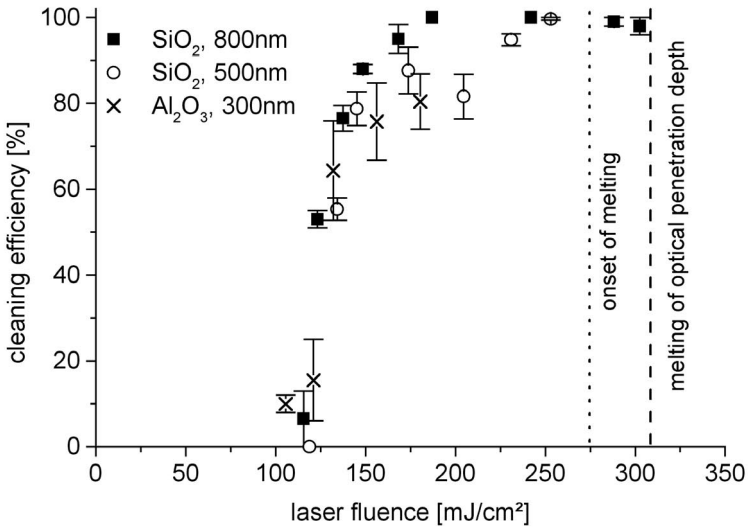

Fig. 27. Experimentally determined cleaning efficiencies as a function of applied laser fluence for particles of different geometry, material and size. A material- and size independent threshold and a steep increase of the cleaning efficiency was monitored.

4.2. Discussion and concluding remarks

Whereas the majority of publications on "laser cleaning" deal with DLC, only few focus on the quantitative determination of removal efficiencies in SLC and the investigation of the basic processes. Before discussing our results described in the previous sections, we will highlight three of these SLC studies in order to provide the necessary background.

In a recent theoretical study (Lu, 1999) have developed a first approximate scenario for the SLC process. The most important prediction of this treatment is size dependent cleaning threshold fluence for the removal of particles from surfaces when using ethanol and acetone as liquids in the process. Experimental results reported by (She, 1999) seem to indicate that the predictions by Lu et al. are valid. Removing Al_2O_3 - particles from NiP surfaces and using a "micron thick" water film, She, Kim and Grigoropoulos found that "the minimum laser fluence for removal of micron-sized or larger contaminants was lower by a factor of about 2 than the fluence necessary for complete removal of 0.3 μm particles".

The second theoretical description of SLC by Wu, Sacher and Meunier, 2000 also predicts a particle size dependent cleaning threshold. As in the Lu model, the authors compute the pressure of a shock wave created by the nucleating bubbles and deduce from this pressure the cleaning force exerted on the contaminant particles. Interestingly the authors report some experimental values. They found that for SiO_2 and Al_2O_3 particles with a mean diameter of 100 nm the particle removal threshold is identical and very close to the threshold of bubble nucleation.

Our findings of a universal cleaning threshold in SLC are in serious contradiction to the predictions of size dependent thresholds. The universality actually refers to two aspects. First we noted an independence of the applied particle materials PS, SiO_2 and Al_2O_3 that was also reported by Wu et al. Even more surprising, however, is the size independence, especially if one brings to mind the large differences in the adhesion forces of the particles used in our experiments. The difference in adhesion between the smallest particles with 60 nm in diameter and the largest ones with a diameter of 800 nm should vary by one order of magnitude, since the adhesion force is proportional to the particle radius (Johnson, 1971; Heim, 1999).

Although the investigations presented here are the first systematic quantitative studies of cleaning thresholds in SLC, many open questions still have to be answered prior to a full understanding of the processes underlying particle removal in SLC. Most of these refer to the dependence of the cleaning threshold and maybe its uniformity on process parameters such as liquid film thickness, liquid composition or laser wavelength. For instance one possible explanation for the different findings of the Grigoropoulos group may be their film thickness of a few micron compared to our 200-400 nm thick films.

The importance of controlling the liquid film properties and understanding its influence on the SLC process becomes even more obvious taking into account that the mechanism considered to be responsible for particle removal - the explosive liquid evaporation - should depend critically on the liquid film properties. As already mentioned above Wu et al. point out a close agreement of the particle removal threshold and the bubble nucleation threshold in their experiments. Indeed such an agreement provides one possible explanation for the universality of the cleaning threshold for particles completely embedded in the liquid film (Mosbacher, 2000). Should SLC be solely governed by an explosion of the liquid film, the process consequently will be determined by parameters of the film rather than particle properties.

Although this is a possible and plausible interpretation of our results, still a lot of research has to be carried out in the field of laser induced bubble nucleation and explosive film evaporation in order to unequivocally clarify the relevant SLC processes. The experiments reported in the first part of this paper were also motivated by this requirement. Improving techniques such as Scattered Light Probes (SLP) and developing powerful tools like Surface Plasmon Probe (SPP) we have been able to elucidate crucial details of laser induced bubble nucleation on surfaces. These include the recording of the pressure waves and detecting the associated pressure amplitudes in the MPa regime. From the experiments we were also able to deduce the gas bubbles growth velocities, which were found to be in the range of a few m/s.

Probably the most important results, however, are related to the measurement of the laser threshold fluences necessary for bubble nucleation and especially the related superheating temperatures of the liquids. Superheating of the liquid can occur in SLC due to the deposition of the laser energy during a very short time interval of a few ns. Since the pressure amplitudes in SLC depend very strongly on the liquid temperature, the

liquid superheating may be the key parameter of the process. One major finding of our experiments in this field is the strong dependence of the extent of superheating on the surface roughness. On thin metal films only small amounts of superheating in the order of 10-30 K have been measured. In contrast on smooth silicon wafers we measured superheating of about 150 K! Moreover, from these superheating temperatures it was possible to show that the heat does not flow freely from the substrate to the liquid, but is inhibited by the solid-liquid heat resistance described in the case of a silicon-water interface by a heat transfer coefficient of $3 \cdot 10^7$ W/m^{2}K.

These two results - high superheating temperatures on smooth silicon wafers and the existence of a finite temperature jump between substrate and liquid - severely question the predictions of the existing SLC models (Lu, 1999; Wu, 2000). Both models strongly rely on several assumptions whose validity must be challenged against the experimental findings. In reference (Lu, 1999), e.g., the bubble growth velocities are computed using the oversimplified formula (14) and our results on bubble growth and superheating (Yavas, 1997 a) obtained on rough metal films are transferred to the silicon-liquid system, which is clearly invalid. Additionally both groups obtain the temperature of the liquid layer by a numerical computation assuming a perfect heat flow from the substrate into the liquid. This is invalid as well, which can be illustrated by the results of numerical computations we carried out on our own. Inserting not only the correct heat transfer coefficient but also temperature dependent material properties for the liquid and the substrate, our calculations based on the 1D heat equation (Bischof, 1996; Dobler, 2002) show temperature differences of liquid and substrate of about 100 K!

Besides the above comments some even more fundamental questions remain. Both models rely on the assumption that shock or pressure waves produced by the growing bubbles/ growing vapor layer exert the removal force on the particles. However, the details of this scenario are still open .

Is it really a vapor layer, as suggested by Wu, which is responsible for the removal force? Or are a few gas bubbles enough, as it is incorporated in the Lu model? Where are these gas bubbles nucleated - all over the bare silicon surface as Lu suggests? In this case as well as in the assumption of a vapor layer - why is it possible to perform “steam" cleaning just by adsorbing a small amount of liquid at the particle-surface interstice via capillary condensation (Fourrier, 2001; Mosbacher, 2002 a)? Here the above approaches to explain the cleaning mechanism fail. And - related to the last

comment - what is the influence of the film parameters, especially the film thickness on the cleaning process and its theoretical description. Can the results obtained so far on bulk liquid be transferred on liquid films? From our point of view these open questions clearly show that still a lot of experimental work on SLC and its fundamentals has to be carried out and that all models proposed so far should be regarded as a first approximate approach.

Even the experimental results pose questions: The threshold for bubble nucleation by a single Nd: YAG-pulse measured for the silicon/bulk water system is about 80 mJ/cm^2. When compared to the universal cleaning threshold in SLC of 110 mJ/cm^2 there is a difference, which will be the subject of further investigations.

Of course all the results on basic processes like laser induced bubble nucleation are very interesting on their own, however, in the end SLC is intended to become a cleaning method applicable in the semiconductor industry. Considering the unsolved questions raised above one might doubt that there is any hope of developing SLC to be a reliable tool in the near future.

We do not agree and believe, that SLC is extremely promising for the process parameters we used. The existence of the universal cleaning threshold at a laser fluence a factor of three below the melting threshold of bare silicon shows, that it is possible to choose one fixed laser fluence well below the substrate melting fluence to remove particles of a broad size range. Moreover, this is also a considerable advantage in terms of possible applications over DLC, where the threshold is size and material dependent, the removal efficiencies are lower and particles smaller than 100 nm could not be removed (Zapka, 1991; Mosbacher, 1998, 2002 a, b). Thus SLC allows particle removal at lower and therefore safer laser fluences, which is essential for avoiding surface modifications.

In the field of liquid parameters still a lot of systematic research has to be carried out, however, our results with removal efficiencies of 90% for particles 60 nm in diameter show that efficient cleaning is already possible. Thus the basic prerequisite for a real world application of SLC is fulfilled: the process works and suitable process parameters are known. Nevertheless it is not clear whether these parameters are the optimum ones. This optimization will be triggered by the growing knowledge on the fundamentals of SLC and will, together with the investigation of different

substrate materials, provide the field of future research on this exciting topic.

Acknowledgements

This review is result of our scientific collaboration between the University of Konstanz, Germany and Data Storage Institute, Singapore. We thank Dr. Nikita Arnold (Johannes-Kepler-University, Linz, Austria), Dr. Bernd-Uwe Runge, Johannes Graf and Florian Lang (all University of Konstanz) for constructive discussions of the findings of our experiments. Financial support by EU TMR project "Laser Cleaning" (no ERBFMRXCT98 0188) and the Konstanz Center for Modern Optics is gratefully acknowledged. Wacker Siltronic supplied the industrial silicon wafers.

References

Assendel'ft E. Y., Beklemyshev V. I., Makhonin I. I., Petrov Yu. N., Prokhorov A. M., Pustovoy V. I., *Optoacoustic effect on the desorption of microscopic particles from a solid surface into a liquid*. Sov. Tech. Phys. Lett., vol. **14**(6), pp. 444-445 (1988a)

Assendel'ft E. Y., Beklemyshev V. I., Makhonin I. I., Petrov Yu. N., Prokhorov A. M., Pustovoy V. I., *Photodesorption of microscopic particles from a semiconductor surfaces into a liquid*, Sov. Tech. Phys. Lett., vol. **14**(8), pp. 650-654 (1988b)

Avesisian C. T., *The homogeneous nucleation limit of liquids*, J. Phys. Chem. Ref. Data, **14**, pp. 695-729 (1985)

Bäuerle D., *Laser Processing and Chemistry*, 3^{d} ed., (Springer-Verlag, Berlin, 2000)

Beklemyshev V. I., Makarov V. V., Makhonin I. I., Petrov Yu. N., Prokhorov A. M., Pustovoy V. I., *Photodesorption of metal ions in a semiconductor-water system*, JETP Letters, vol. **46**, pp. 347-350 (1987)

Bischof J., *Metallische Dünnfilmschmelzen nach Pulslaserbestrahlung: Phasenumwandlungen und Instabilitäten*, PhD thesis (Universität Konstanz, 1996)

Boneberg J., *Dynamische Verfestigung von Halbleiterschichten nach ns-Laser-Annealing*, PhD thesis (University of Konstanz, 1993)

Born M., Wolf E., *Principles of Optics*, 7-th Edition, (Cambridge University Press, 1999)

Boughaba S., Wu X., Sacher E., Meunier M., *Liquid explosive evaporative removal of submicron particles from hydrophilic oxidized silicon surface,* J. Adhesion, **61**, pp. 293-307 (1997)

Carey V. P., *Liquid-Vapor Phase Change Phenomena* (Hemisphere Publishing Cooperation, Washington, 1992)

Cerbe G., Hoffmann H. J., *Einführung in die Thermodynamik* (Carl Hanser Verlag, München, 1999)

Cole R., *Boiling nucleation*, Adv. Heat Transfer, **10**, pp. 85-167 (1974)

Debenedetti P. G., *Metastable liquids: Concepts and Principles* (Princeton University Press, Princeton, New Jersey, 1996)

DeJule R., *Trends in wafer cleaning*. Semiconductor International, **8**, pp. 65-68 (1998)

Dobler V., *Dynamische Messungen zum Laser Cleaning*, PhD thesis (University of Konstanz, 2002)

Engelsberg A. C., In: *Surface Chemical Cleaning and Passivation for Semiconductor Processing*, Ed. by G. Higashi, E. Irene, T. Ohmi, Proc. MRS, vol. **315**, p. 255 (1993)

Fourrier T., Schrems G., Mühlberger T., Arnold N., Heitz J., Bäuerle D., Mosbacher M., Boneberg J., Leiderer P., *Laser cleaning of polymer surfaces*, Appl. Phys. A **72**, pp. 1-6 (2001)

Grigull U., Starub J., Schiebner P., *Steam tables in SI-units* (Springer-Verlag, Berlin, Heidelberg, 1984)

Halfpenny D. R., Kane D. M., *A quantitative analysis of single pulse UV dry laser cleaning*, J. Appl. Phys., **86**, pp. 6641-6646 (1999)

Hattori T., Solid State Tech., **8**, July 1990

Heim L.-O., Blum J., Preuss M., Butt H.-J., *Adhesion and friction forces between spherical micrometer-sized particles*, Phys. Rev. Lett, **83** (16), pp. 3328-3331 (1999)

Herminghaus S., Leiderer P., *Surface plasmon enhanced transient thermoreflectance*, Appl. Phys. A **51**, p. 350 (1990)

Hoenig S. A., In: *Particles on Surfaces: Detection, Adhesion and Removal*, Ed. by K. L. Mittal, vol. **1**, p. 3 (Plenum Press, New York, NY, 1988)

Héroux J. B., Boughaba S., Ressejac I., Sacher E., Meunier M., *CO_2 laser-assisted removal of submicron particles from solid surfaces*, J. Appl. Phys., **79**, pp. 2857-2862 (1996)

Imen K., Lee S. J., Allen S. D., *Laser-assisted micron scale particle removal*, Appl. Phys. Lett., **58**, pp. 203-205 (1991)

Johnson K. L., Kendall K., Roberts A. D., *Surface energy and the contact of elastic solids*, Proc. R. Soc. Lond. A, **324**, pp. 301-313 (1971)

Johnson P. B., Christy R. W., Phys. Rev. B, **6**, p. 4370 (1972)

Kagen Y., *The kinetics of boiling of a pure liquid*, Russian J. Phys. Chem., 34, pp. 42-46 (1960)

Kameda M., Yamada M., Matsumoto Y., *Nonlinear oscillation of a small gas bubble*, In: Advances in nolinear acoustics, Ed. by H. Hobaek (World Scientific, 1993)

Katz J. L., Blander M., *Condensation and boiling: Correction to homogeneous nucleation theory for nonideal gases*, J. Colloid Interface Sci., **42**, pp. 496-502 (1973)

Kelley J. D., Hovis F. E., *A thermal detachment mechsnism for particle removal from surfaces by pulsed laser irradiation*, Microelectronic Engineering, **20**, 159-170 (1993)

Kim D., Park H. K., Grigoropoulos C. P., *National Heat Trans. Conf. Proc*., **4**, p. 69 (1996)

Kohli R., In: *Particles on Surfaces*, Ed. by K. L. Mittal (VSP Publishing, 2002)

Kretschmann E., Raether H., *Z. Naturf. A*, **23**, p. 2135 (1968)

Kurz H., Lompre L. A., Liu J. M., J. de Physique, **10** (44), C5-23 (1983)

Leiderer P., Boneberg J., Dobler V., Mosbacher M., Münzer H.-J., Chaoui N., Siegel J., Solis J., Afonso C. N., Fourrier T., Schrems G., Bäuerle D., *Laser-induced particle removal from silicon wafers*, Proc. SPIE, vol. **4065**, pp. 249-259 (2000)

Leiderer P., Boneberg J., Mosbacher M., Schilling A., Yavas O., *Laser cleaning of silicon surfaces*, Proc. SPIE, vol. **3274**, pp. 68-77 (1998)

Lowndes D. H., Wood R. F., Westbrook R. D., *Pulsed neodymium: yttrium aluminum garnet laser (532 nm) melting of crystalline silicon: Experiment and theory*, Appl. Phys. Lett., **43** (3), pp. 258-260 (1983)

Lu Y. F., Zhang Y., Wan Y. H., Song W. D., *Laser cleaning of silicon surfaces with deposition of different liquid films*, Appl. Surf. Sci., **138-139**, pp. 140-144 (1999)

Lu Y. F., Zheng Y. W., Song W. D., *Laser induced removal of spherical particles from silicon wafers*, J. Appl. Phys. **87**, pp. 1534-1539 (2000a)

Lu Y. F., Zhang L., Song W. D., Zheng Y. W., Luk'yanchuk B. S., *Laser writing of sub-wavelength structure on silicon (100) surfaces with particle enhanced optical irradiation,* JETP Letters, vol. **72**, pp. 457-459 (2000 b)

Lu Y. F., Zhang L.**,** Song W. D., Zheng Y.W., Luk`yanchuk B. S., *Particle-Enhanced Near-Field Optical Effect and Laser Writing for Nanostructure Fabrication,* Proc. SPIE, vol. **4426**, pp.143-145 (2002)

Luk'yanchuk B. S., Zheng Y. W., Lu Y. F., *Laser Cleaning of the surface: Optical resonance and near-field effects*, Proc. SPIE, vol. **4065**, pp. 576-587 (2000)

Luk'yanchuk B. S., Zheng Y. W., Lu Y. F., *Basic physical problems related to dry laser cleaning*, RIKEN Review No. 43, pp. 47-65 (2002)

Matsumoto Y., Takemura F., *Numerical analysis on a bubble motion with full equations*, In: M. F. Hamilton, D. T. Blackstock (Eds.), Frontiers of nonlinear acoustics: Proceedings of the 12th ISNA, (Elsevier Science Publishers, London, 1990)

Matsumoto Y., Kameda M., Takemura F., Ohashi H., *Numerical simulations of pressure wave behaviors in bubbly liquids*, In: G. Matsui, A. Serizawa, Y. Tsuji (Eds.), Proceedings of the International Conference on Multiphase Flows, pp. 327-330 (1991 a)

Matsumoto Y., Takemura F., Kameda M., *Bubble motion in an oscillatory pressure field*, In: H. Kato, O. Furuya (Eds.), "Cavitation' 91", The first ASME-JSME Fluid Engineering Conference, vol. **116**, pp. 33-38 (The American Society of Mechanical Engineers, 1991 b)

Mosbacher M., Dobler V., Boneberg J., Leiderer P., CPD 2.12. In CLEO/Europe - EQEC, (1998)

Mosbacher M., Chaoui N., Siegel J., Dobler V., Solis J., Boneberg J., Afonso C. N., Leiderer P., *A comparison of ns and ps steam laser cleaning of Si surfaces*, Appl. Phys. A, **69** [Suppl.], pp. 331-334, (1999)

Mosbacher M., Dobler V., Boneberg J., Leiderer P., *Universal threshold for the steam laser cleaning of submicron spherical particles from silicon* , Appl. Phys. A, **70**, pp. 669-672 (2000)

Mosbacher M., Münzer H.-J., Zimmermann J., Solis J., Boneberg J., Leiderer P., *Optical field enhancement effects in laser-assisted particle removal*, Appl. Phys. A, **72**, (2001)

Mosbacher M., Bertsch M., Münzer H.-J., Dobler V., Runge B.-U., Bäuerle D., Boneberg J., Leiderer P., *Laser cleaning of silicon wafers* -

mechanisms and efficiencies, Proc. SPIE, vol. **4426**, pp. 308-314 (2002 a)

Mosbacher M., Münzer H.-J., Bertsch M., Dobler V., Chaoui N., Siegel J., Oltra R., Bäuerle D., Boneberg J., Leiderer P., *Laser assisted particle removal from silicon wafers*, In: "Particles on Surfaces", Ed. by K. L. Mittal (VSP Publishing, 2002 b)

Münzer H.-J., Mosbacher M., Bertsch M., Dubbers O., Burmeister F., Pack A., Wannemacher R., Runge B.-U., Bäuerle D., Boneberg J., Leiderer P., *Optical near field effects in surface nanostructuring and laser cleaning, Proc. SPIE*, vol. **4426**, pp. 180-183 (2002)

Park H. K., Grigoropoulos C. P., Leung W. P., Tam A. C., *A practical excimer laser-based cleaning tool for removal of surface contaminants*, IEEE Transactions on Components, Packaging, and Manufacturing Technology A, **17** (4), pp. 631-643 (1994 a)

Park H. K., Grigoropoulos C. P., Poon C. C., Tam A. C., Yavas O., Leiderer P., *Optical probing of the temperature and pressure transients at a liquid/solid interface due to pulsed laser-induced vaporization*, Proc. SPIE, vol. **2498**, pp. 32-40 (1994 b)

Park H. K., Grigoropoulos C. P., Poon C. C., Tam A. C., *Optical probing of the temperature transients during pulsed laser-induced boiling of liquids*, Appl. Phys. Lett., **68**, pp. 596-598 (1996 a)

Park H. K., Kim D., Grigoropoulos C. P., *Pressure generation and measurement in the rapid vaporization of water on a pulsed-laser-heated substrate*, J. Appl. Phys., **80**, pp. 4072-4081 (1996 b)

Schiebener P., Straub J., Levelt-Sengers J. M. H., Gallagher J. S., J. Phys. Chem. Ref. Data, **19**, p. 677 (1990)

Schilling A., Yavas O., Bischof J., Boneberg J., Leiderer P., *Absolute pressure measurements on a nanosecond time scale using surface plasmons*, Appl. Phys. Lett., **69**, pp. 4159-4161 (1996)

Sematech Inc., *International technology roadmap for semiconductors* (Technical report, 2000), http://public.itrs.net/

She M., Kim D. S., Grigoropoulos C. P., *Liquid-assisted pulsed laser cleaning using near-infrared and ultraviolet radiation*, J. Appl. Phys., **86** (11), pp. 6519-6524 (1999)

Skripov V. P., *Metastable liquids* (Halsted Press, John Wiley & Sons, New York, 1974)

Skripov V. P., Sinitsyn E. N., Pavlov P. A., Ermakov G. V., Muratov G. N., Bulanov N. V., Badakov V. G., *Thermophysical properties of liquids in*

the metastable (superheated) state (Gordon and Breach, New York, 1988)

Swartz E. T., Pohl R. O., *Thermal boundary resistance*, Rev. Mod. Phys., **61**, pp. 605-668 (1989)

Tam A. C., Leung W. P., Zapka W., Ziemlich W., *Laser-cleaning techniques for removal of surface particulates*, J. Appl. Phys., **71** (7), pp. 3515-3523 (1992)

Tam A. C., Leung W. P., Zapka W., In: *Particles on surfaces*, Ed. by K. L. Mittal, pp. 405-418 (Marcel Dekker, New York, 1995)

Tam A. C., Park H. K., Grigoropoulos C. P., *Laser cleaning of surface contaminants*, Appl. Surf. Sci., **127-129**, pp. 721-725 (1998)

Tong L. S., Tang Y. S., *Boiling heat transfer and two-phase flow* (Taylor & Francis, Washington, 1997)

Vereecke G., Röhr E., Heyns M. M., *Laser-assisted removal of particles on silicon wafers*, J. Appl. Phys., **85** (7), pp. 3837-3843 (1999)

Wagner W., Cooper J. R., Dittmer A., Kijima, Kretzschmar H.-J., Kruse A., Mares R., Oguchi K., Sato H., Stöcker I., Sifner O., Takaishi Y., Tanishita I., Trübach J., Willkommen T., *The IAPWS industrial formulation 1997 for the thermodynamic properties of water and steam*, ASME Trans., **122**, pp. 150-182 (2000)

Wu X., Sacher E., Meunier M., *The modeling of excimer laser particle removal from hydrophilic silicon surfaces*, J. Appl. Phys., **87** (8), pp. 3618-3627 (2000)

Yavas O., Leiderer P., Park H. K., Grigoropoulos C. P., Poon C. C., Leung W. P., Do N., Tam A. C., *Optical reflectance and scattering studies of nucleation and growth of bubbles at a liquid-solid interface induced by pulsed laser heating*, Phys. Rev. Lett., **70** (12), pp. 1830-1833 (1993)

Yavas O., *Laserinduzierte Gasblasennukleation*, PhD thesis (University of Konstanz, 1994 a)

Yavas O., Leiderer P., Park H. K., Grigoropoulos C. P., Poon C. C., Leung W. P., Do N., Tam A. C., *Optical and acoustic study of nucleation and growth of bubbles at a liquid-solid interface induced by nanosecond-pulsed-laser heating*, Appl. Phys. A, **58**, pp. 407-415 (1994 b)

Yavas O., Leiderer P., Park H. K., Grigoropoulos C. P., Poon C. C., Tam. A.C. , *Enhanced acoustic cavitation following laser-induced bubble formation: long-term memory effect*, Phys. Rev. Lett., **72**, pp. 2021-2024 (1994 c)

Yavas O., Schilling A., Bischof J., Boneberg J., Leiderer P., *Bubble nucleation and pressure generation during laser cleaning of surfaces*, Appl. Phys. A, **64**, pp. 331-339 (1997 a)

Yavas O., Schilling A., Bischof J., Boneberg J., Leiderer P., *Study of nucleation process during laser cleaning of surfaces*, Laser Physics, **7**, pp. 343-348 (1997 b)

Zapka W., Ziemlich W., Tam A.C., *Efficient pulsed laser removal of 0.2 μm sized particles from a solid surface*, Appl. Phys. Lett., **58** (20), pp. 2217-2219 (1991)